

C 13.46:1001



NBS TECHNICAL NOTE 1001



U.S. DEPARTMENT OF COMMERCE / National Bureau of Standards

Laser Far-Field Beam-Profile Measurements By The Focal Plane Technique

NATIONAL BUREAU OF STANDARDS

The National Bureau of Standards¹ was established by an act of Congress March 3, 1901. The Bureau's overall goal is to strengthen and advance the Nation's science and technology and facilitate their effective application for public benefit. To this end, the Bureau conducts research and provides: (1) a basis for the Nation's physical measurement system, (2) scientific and technological services for industry and government, (3) a technical basis for equity in trade, and (4) technical services to promote public safety. The Bureau consists of the Institute for Basic Standards, the Institute for Materials Research, the Institute for Applied Technology, the Institute for Computer Sciences and Technology, the Office for Information Programs, and the Office of Experimental Technology Incentives Program.

THE INSTITUTE FOR BASIC STANDARDS provides the central basis within the United States of a complete and consistent system of physical measurement; coordinates that system with measurement systems of other nations; and furnishes essential services leading to accurate and uniform physical measurements throughout the Nation's scientific community, industry, and commerce. The Institute consists of the Office of Measurement Services, and the following center and divisions:

Applied Mathematics — Electricity — Mechanics — Heat — Optical Physics — Center for Radiation Research — Laboratory Astrophysics² — Cryogenics² — Electromagnetics² — Time and Frequency².

THE INSTITUTE FOR MATERIALS RESEARCH conducts materials research leading to improved methods of measurement, standards, and data on the properties of well-characterized materials needed by industry, commerce, educational institutions, and Government; provides advisory and research services to other Government agencies; and develops, produces, and distributes standard reference materials. The Institute consists of the Office of Standard Reference Materials, the Office of Air and Water Measurement, and the following divisions:

Analytical Chemistry — Polymers — Metallurgy — Inorganic Materials — Reactor Radiation — Physical Chemistry.

THE INSTITUTE FOR APPLIED TECHNOLOGY provides technical services developing and promoting the use of available technology; cooperates with public and private organizations in developing technological standards, codes, and test methods; and provides technical advice services, and information to Government agencies and the public. The Institute consists of the following divisions and centers:

Standards Application and Analysis — Electronic Technology — Center for Consumer Product Technology: Product Systems Analysis; Product Engineering — Center for Building Technology: Structures, Materials, and Safety; Building Environment; Technical Evaluation and Application — Center for Fire Research: Fire Science; Fire Safety Engineering.

THE INSTITUTE FOR COMPUTER SCIENCES AND TECHNOLOGY conducts research and provides technical services designed to aid Government agencies in improving cost effectiveness in the conduct of their programs through the selection, acquisition, and effective utilization of automatic data processing equipment; and serves as the principal focus within the executive branch for the development of Federal standards for automatic data processing equipment, techniques, and computer languages. The Institute consist of the following divisions:

Computer Services — Systems and Software — Computer Systems Engineering — Information Technology.

THE OFFICE OF EXPERIMENTAL TECHNOLOGY INCENTIVES PROGRAM seeks to affect public policy and process to facilitate technological change in the private sector by examining and experimenting with Government policies and practices in order to identify and remove Government-related barriers and to correct inherent market imperfections that impede the innovation process.

THE OFFICE FOR INFORMATION PROGRAMS promotes optimum dissemination and accessibility of scientific information generated within NBS; promotes the development of the National Standard Reference Data System and a system of information analysis centers dealing with the broader aspects of the National Measurement System; provides appropriate services to ensure that the NBS staff has optimum accessibility to the scientific information of the world. The Office consists of the following organizational units:

Office of Standard Reference Data — Office of Information Activities — Office of Technical Publications — Library — Office of International Standards — Office of International Relations.

¹ Headquarters and Laboratories at Gaithersburg, Maryland, unless otherwise noted; mailing address Washington, D.C. 20234.

² Located at Boulder, Colorado 80302.

Laser Far-Field Beam-Profile Measurements By The Focal Plane Technique

G.W. Day
C.F. Stubenrauch

Electromagnetic Division
Institute for Basic Standards
National Bureau of Standards
Boulder, Colorado 80303



DEMCO

U.S. DEPARTMENT OF COMMERCE, Juanita M. Kreps, Secretary

Sidney Harman, Under Secretary
Jordan J. Baruch, Assistant Secretary for Science and Technology

NATIONAL BUREAU OF STANDARDS, Ernest Ambler, Director

Issued March 1978

NATIONAL BUREAU OF STANDARDS TECHNICAL NOTE 1001
Nat. Bur. Stand. (U.S.), Tech. Note 1001, 52 pages (Mar 1978)
CODEN: NBTNAE

U.S. GOVERNMENT PRINTING OFFICE
WASHINGTON: 1978

For sale by the Superintendent of Documents, U.S. Government Printing Office, Washington, D.C. 20402

Stock No. 003-003-01902-0 Price \$2.20 (Add 25 percent additional for other than U.S. mailing)

CONTENTS

	<u>Page</u>
1. INTRODUCTION-----	1
2. BASIC RELATIONSHIPS-----	2
2.1 Propagation Laws-----	2
2.2 Transform Properties of a Focusing Element-----	5
2.3 Approximations-----	7
2.4 Equivalence-----	8
3. THE QUESTION OF DEFINITION-----	8
3.1 Single Transverse Modes-----	8
3.2 Multimode Beams-----	10
4. SELECTION OF FOCUSING ELEMENT-----	11
4.1 Refracting Elements-----	11
4.1.1 Single Element Lenses-----	11
4.1.2 Multi-element and Aspheric Lenses-----	16
4.2 Reflecting Elements-----	16
4.2.1 Parabolic Mirrors-----	16
4.2.2 Spherical Mirrors-----	16
5. ESTIMATION OF CERTAIN ERROR SOURCES-----	20
5.1 Computational Technique-----	20
5.2 The Fresnel Approximation-----	22
5.3 Lens Aberration-----	22
5.4 The Position of the Observation Plane-----	25
5.5 Summary of Computations-----	28
6. EXPERIMENTAL IMPLEMENTATION-----	29
6.1 Characterizing the Focusing Element-----	29
6.1.1 Lenses-----	29
6.1.2 Mirrors-----	33
6.2 Other Experimental Considerations-----	37
7. SPATIALLY RESOLVED MEASUREMENTS-----	39
8. SUMMARY-----	41
9. REFERENCES-----	41
10. ACKNOWLEDGMENT-----	42
APPENDIX-----	43

LASER FAR-FIELD BEAM-PROFILE MEASUREMENTS
BY THE FOCAL PLANE TECHNIQUE

An analysis of laser far-field beam-profile measurements by the focal plane technique is given. Particular attention is paid to systems at $\sim 1\mu\text{m}$ wavelength and having apertures up to 10 cm. The basic mathematics is reviewed and approximations are evaluated. Using geometrical optics techniques, it is shown that an $f/20$ plano-convex lens is an appropriate choice for the focusing element. For two arbitrarily chosen laser beam profiles the errors associated with the choice of this lens are discussed through the use of computed far-field and focal-plane irradiance distributions. Experimental procedures including methods of testing the optical elements are also given.

Key words: Beam divergence; beam profile; lasers; optical propagation.

1. INTRODUCTION

The accelerating use of pulsed lasers for ranging, target designation, and similar applications where maximizing the radiation on a distant target is desired leads to the need for methods of accurately characterizing beam profiles. The Q-switched Nd:YAG laser emitting intense $1.06\mu\text{m}$ wavelength pulses of 20-30 ns duration and low repetition rate ($\sim 10\text{ Hz}$) is typical of the sources used in these applications. Beam profiles at the source are generally complex and vary from pulse to pulse. Moderately large optics ($\sim 10\text{ cm}$) are used to obtain beam divergence in the range of 10^{-4} to 10^{-2} radians.

For such a source the far-field pattern is only observed beyond several thousand meters from the source. Thus direct measurement is not generally possible, and some form of near-field to far-field transformation technique must be applied. By transformation technique we mean a method whereby the far-field patterns can be determined by measurements taken relatively close to the source.

Given the complex amplitude distribution of the field across a plane near the source, one can, in principle, compute the far-field distribution from diffraction theory. The relationship, as shown in a later section, is essentially that of a Fourier transform.

In antenna measurements, where similar problems arise in obtaining far-field patterns, it is common to measure the complex field amplitude and compute the far-field pattern using fast Fourier transform algorithms. At optical wavelengths, however, two problems make this approach difficult. First, experimental determination of the complex amplitude distribution is difficult in this region of the spectrum, especially for pulsed sources. Second, the amount of data required (that is, the grid spacing over which data are taken) is inversely related to the wavelength. At optical wavelengths the volume of data processing becomes prohibitive.

A second approach is to use the fact that the field distribution in the focal plane of a lens or mirror is related to the far-field distribution. It is useful to think of the focusing element as simply a means of information processing analogous to that described in the preceding paragraph. An analysis of this technique and its experimental implementation are the primary subjects of this document. The mathematical background is reviewed in section 2 with attention to necessary approximations. Section 3 discusses some questions of definition, relative to beam characterization. Sections 4 and 5 analyze the limitations of the technique from both a geometrical and physical optics perspective. Section 6 deals with experimental implementation and section 7 with possible extensions of the technique.

It should be pointed out here that in most cases determining the intrinsic propagation characteristics of a laser is only the first step in determining the actual irradiance distribution on a distant target. If propagation is through the atmosphere, the beam may be disturbed by turbulence, scattering, thermal defocusing (blooming) and other effects.

Determining the intrinsic propagation characteristics is, however, a necessary first step and should aid an investigation of the complete propagation problem.

2. BASIC RELATIONSHIPS

2.1 Propagation Laws

The purpose of this section is to draw together some of the basic expressions governing the propagation of electromagnetic radiation and observe their application to the specific problem of determining the propagation characteristics of laser radiation. The basic problem is that given a field distribution over some surface in space (usually a plane), one wishes to learn the field distribution over a second surface a distance away. Each polarization is assumed to be independent and is characterized by a complex scalar amplitude function.

It has become popular to proceed [1,2,3] by recognizing that the source distribution can be represented as a linear superposition of plane wave solutions to the scalar wave equation. Through the use of the Fourier transform, the source distribution is decomposed into plane wave components, each of which is assumed to propagate independently to the observation plane where they are recombined. Such a procedure is fully analogous to frequency domain solutions of electronic circuit problems.

The mechanics of the procedure are as follows:

1. The two-dimensional Fourier transform of a complex source distribution, U_1 , is given by

$$\hat{U}_1(\xi, \eta) = F\{U_1(x_1, y_1)\} = \iint_{-\infty}^{\infty} U_1(x_1, y_1) e^{-i2\pi(x_1\xi + y_1\eta)} dx_1 dy_1 \quad (2-1)$$

where x_1 and y_1 are the spatial variables in the source plane and ξ and η are the transform variables.

2. The Fourier transform is recognized as a decomposition of $U_1(x_1, y_1)$ into plane wave components of the form

$$e^{-i2\pi(ft - \xi x - \eta y - \zeta z)}$$

The time dependence is normally dropped and propagation nominally along the z direction is assumed. The z dependence is then understood from the relation

$$\xi^2 + \eta^2 + \zeta^2 = \frac{1}{\lambda^2}.$$

This leaves

$$e^{i2\pi(\xi x + \eta y)}$$

with values of ξ and η (called spatial frequencies) giving the direction of propagation of the component through

$$\xi = \frac{\sin \theta}{\lambda}, \quad \eta = \frac{\sin \phi}{\lambda}$$

where θ and ϕ are the angles between the direction of propagation of the plane wave component and the y - z and x - z planes, respectively. Note that ξ and η take values from $-1/\lambda$ to $+1/\lambda$. The Fourier transform of the function $U(x, y)$ is thus commonly called its plane wave spectrum.

3. In propagating a distance, d , along the z axis through free space each plane wave undergoes a phase shift of the form

$$e^{ikd(1-\lambda^2\xi^2-\lambda^2\eta^2)^{\frac{1}{2}}} \quad (2-2)$$

as shown in figure 2-1.

4. Thus if one multiplies the plane wave spectrum (2-1) in the x_1, y_1 plane by the propagation factor (2-2) one obtains the plane wave spectrum in the x_2, y_2 plane at $z = d$.

$$\hat{U}_2(\xi, \eta) = \hat{U}_1(\xi, \eta) e^{ikd(1-\lambda^2\xi^2-\lambda^2\eta^2)^{\frac{1}{2}}}.$$

5. The resulting amplitude function is then given by the inverse transform

$$\begin{aligned} U_2(x_2, y_2) &= F^{-1}\{\hat{U}_2(\xi, \eta)\} \\ &= \iint \hat{U}_2(\xi, \eta) e^{+i2\pi(x_2\xi+y_2\eta)} d\xi d\eta. \end{aligned}$$

Analysis of this form leads to a derivation of the Fresnel-Kirchhoff diffraction integral

$$U_2(x_2, y_2) = \frac{d}{i\lambda} \int_{-\infty}^{\infty} \int_{-\infty}^{\infty} U_1(x_1, y_1) \frac{\exp\{ik[d^2+(x_2-x_1)^2+(y_2-y_1)^2]^{\frac{1}{2}}\}}{[d^2+(x_2-x_1)^2+(y_2-y_1)^2]} dx_1 dy_1. \quad (2-3)$$

The steps leading to this expression are somewhat mathematically complex and are summarized in the appendix.

It is common to consider cases where x and y are small enough relative to d that the exponential term can be written as $\exp(ikd) \exp\{ik[(x_2-x_1)^2 + (y_2-y_1)^2]/2d\}$ which leads to

$$\begin{aligned} U_2(x_2, y_2) &= \frac{1}{i\lambda d} e^{ikd} e^{ik \frac{x_2^2+y_2^2}{2d}} \\ &\times \iint U_1(x_1, y_1) e^{ik \frac{x_1^2+y_1^2}{2d}} e^{-ik \frac{x_1x_2+y_1y_2}{d}} dx_1 dy_1. \end{aligned} \quad (2-4)$$

If x_1 and y_1 are so small relative to d such that the first exponential term within the integral may be neglected, the expression (2-4) becomes:

$$\begin{aligned} U_2(x_2, y_2) &= \frac{1}{i\lambda d} e^{ikd} e^{ik \frac{x_2^2+y_2^2}{2d}} \\ &\times \iint U_1(x_1, y_1) e^{-ik \frac{x_1x_2+y_1y_2}{d}} dx_1 dy_1. \end{aligned} \quad (2-5)$$

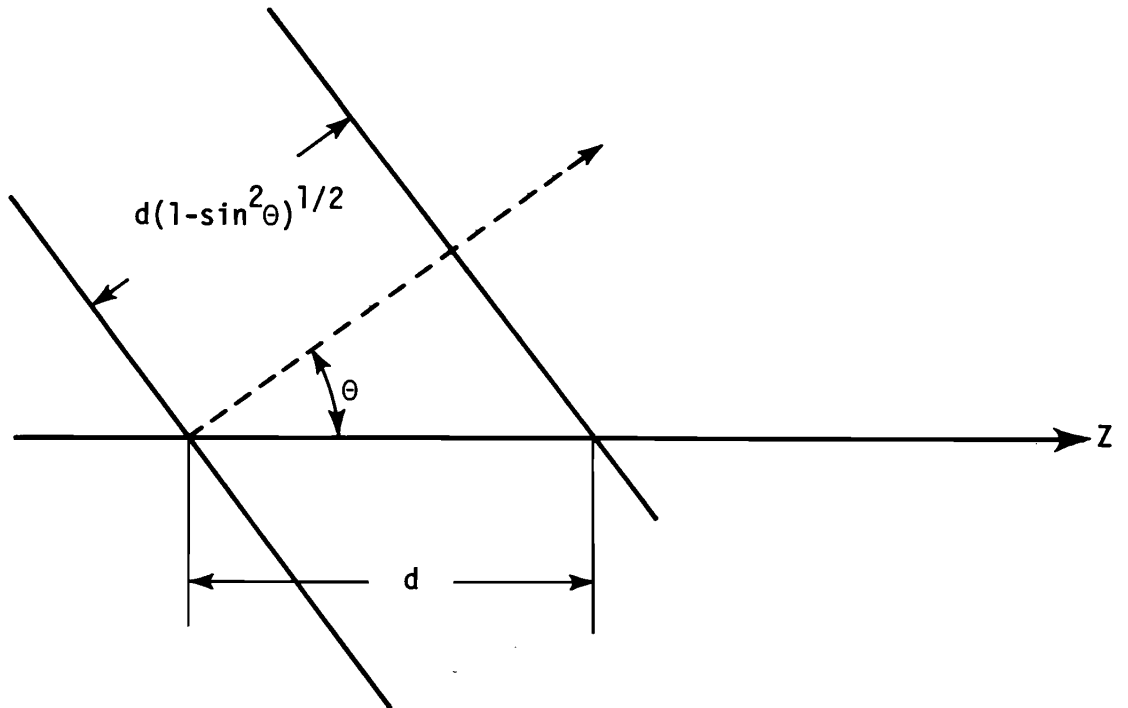


Figure 2-1. Propagation of a plane wave component a distance d in the z direction occurs for propagation a distance $d(1-\sin^2\theta)^{1/2}$ along the wave normal. The phase shift undergone by each component is $\exp ikd(1-\lambda^2\xi^2)^{1/2}$ or $\exp ikd(1-\lambda^2\xi^2-\lambda^2\eta^2)^{1/2}$ in three dimensions.

That region where expression (2-4) is appropriate is commonly called the Fresnel region while the region where (2-5) applies is called the far-field or Fraunhofer region. The transition between these regions is generally taken to be about $d = \frac{D^2}{\lambda}$ where D is the diameter over which U_1 is non-zero. At this distance, d , the maximum on axis phase error from neglecting this term is $\lambda/8$. For a 10 cm diameter source at 10^{-4} cm wavelength, expression (2-5) applies by this definition for distances greater than 10^4 meters.

Examination of (2-5) shows that except for the phase and scaling factors preceding the integral it simply represents a Fourier transform of the source function. The transform variables are identified as $\frac{x_2}{\lambda d}$ and $\frac{y_2}{\lambda d}$. The phase factors imply that the transform lies on a spherical surface of radius d , rather than a plane at $z = d$. This distinction is not generally significant and disappears completely when intensity measurements (that is UU^*) are made.

2.2 Transform Properties of a Focusing Element

As stated in the Introduction it is possible to observe the far-field distribution much closer to the source through the use of a focusing element. In order to indicate the conditions under which this is true, we provide the following analysis [4].

Consider figure 2-2, which shows a lens inserted between the source plane and the observation plane, at distances d_1 and d_2 , respectively, from the two planes. For present purposes we assume that the lens introduces a phase factor of

$$P(x,y) = e^{-ik\left(\frac{x^2+y^2}{2f}\right)}$$

and that it is sufficiently large that its aperture is not important.

Using the Fresnel approximation (2-4) the complex amplitude function in the plane of the lens is

$$U_2(x_2, y_2) = \frac{1}{i\lambda d_1} e^{ikd_1} h(x_2, y_2; d_1) \times \iint U_1(x_1, y_1) h(x_1, y_1; d_1) \exp[ik(x_1 x_2 + y_1 y_2)/2d_1] dx_1 dy_1 \quad (2-6)$$

where the notation $h(x,y;d) = e^{ik\frac{x^2+y^2}{2d}}$ is used for simplicity.

The distribution $U_3(x_3, y_3)$ is given in terms of $U_2(x_2, y_2)$ as

$$U_3(x_3, y_3) = \frac{e^{ikd_2}}{i\lambda d_2} h(x_3, y_3; d_2) \times \iint U_2(x_2, y_2) P(x_2, y_2) h(x_2, y_2; d_1) \times e^{\frac{-ik(x_2 x_3 + y_2 y_3)}{2d}} dx_2 dy_2. \quad (2-7)$$

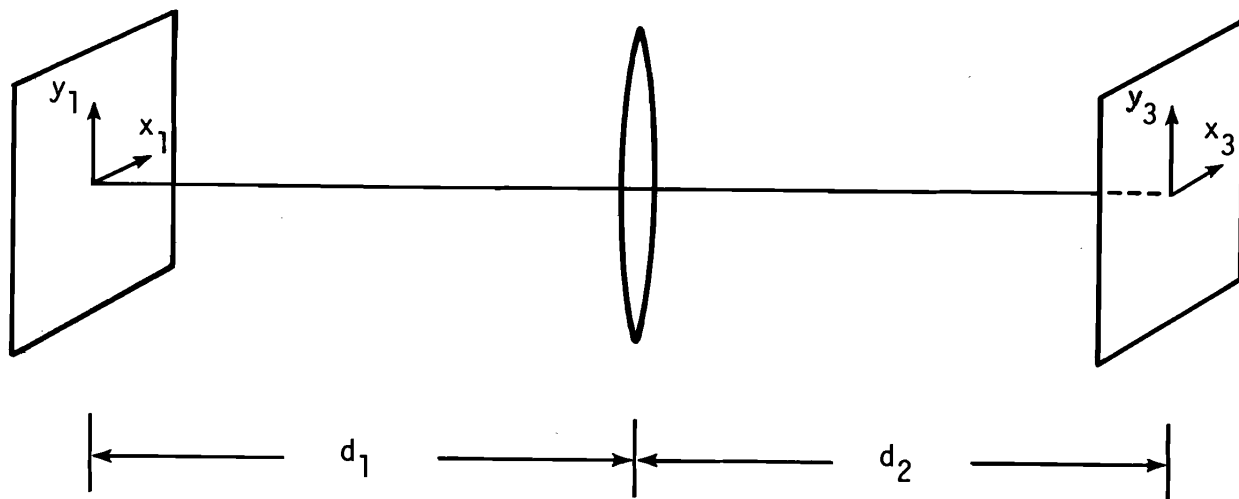


Figure 2-2. Geometry for demonstrating the Fourier transforming properties of lenses. The lens is assumed to have zero thickness and a phase factor $\exp -ik(x_2^2 + y_2^2)/2f$, where the x_2, y_2 plane is that of the lens.

Substituting (2-6) into (2-7), changing the order of integration, and evaluating the integral over x_2 and y_2 yields

$$\begin{aligned}
 U_3(x_3, y_3) = & \frac{w}{i\lambda d_1 d_2} \exp\left(\frac{ik}{2d_2} (x_3^2 + y_3^2) \left(1 - \frac{w}{d_2}\right)\right) \\
 & \times \iint U_1(x_1, y_1) \exp\left(\frac{ik}{2d_1} (x_1^2 + y_1^2) \left(1 - \frac{w}{d_1}\right)\right) \\
 & \times \exp\left(-ik(x_1 x_3 + y_1 y_3) \frac{w}{d_1 d_2}\right) dx_1 dy_1
 \end{aligned} \tag{2-8}$$

where

$$\frac{1}{w} \equiv \frac{1}{d_1} + \frac{1}{d_2} - \frac{1}{f}.$$

By specializing to the case where $w = d_1$, which gives $d_2 = f$, we find a Fourier transform relationship between the x_1, y_1 plane and the x_3, y_3 plane.

$$\begin{aligned}
 U_3(x_3, y_3) = & \frac{1}{i\lambda f} \exp\left(\frac{ik}{2f} (x_3^2 + y_3^2) \left(1 - \frac{d_1}{f}\right)\right) \\
 & \times \iint U_1(x_1, y_1) \exp\left\{-ik\left(\frac{x_1 x_3}{f} + \frac{y_1 y_3}{f}\right)\right\} dx_1 dy_1
 \end{aligned} \tag{2-9}$$

The transform variables are seen to be $\frac{x_3}{\lambda f}$ and $\frac{y_3}{\lambda f}$. The phase factor preceding the integral disappears for $d_1 = f$, that is, the Fourier transform thus derived contains no phase error if the source and observation planes are each located one focal length from the focusing element. If this condition is not satisfied, the transform contains a spherical phase error. In experiments where only intensity, UU^* , is detected the phase error, as in the case of the far-field expression, is of no consequence.

2.3 Approximations

It is important to summarize, at this point, the approximations made in reaching equation (2-9). In addition to the use of scalar theory we have assumed the following:

1. That the approximations leading to the Fresnel form of the diffraction integral are valid. Essentially this means that terms like $[d^2 + (x_2 - x_1)^2 + (y_2 - y_1)^2]^{\frac{1}{2}}$ can be approximated by $d + [(x_2 - x_1)^2 + (y_2 - y_1)^2]/2d$, even in exponentials where the approximation represents a phase error.
2. That the effect of the focusing element can be adequately represented by the phase factor $\exp -ik[(x^2 + y^2)/2f]$. This basically implies that the focusing element converts plane wavefronts into parabolic wavefronts instead of spherical wavefronts which would be obtained if the phase factor of a perfect lens, $\exp -ik[(f^2 + x^2 + y^2)^{\frac{1}{2}} - f]$, were used.

For the wavelength and dimensions we expect to use here, these approximations can be shown to be marginally valid. However, due to the fact that these terms appear with opposite sign in exponents the combined effect of the two approximations is much less than either alone. This is verified by numerical computation in section 5.

2.4 Equivalence

Acceptance of equation (2-9) and a comparison of it with expression (2-5) form the basis for the use of a focusing element to obtain far-field distributions. The intensity functions calculated from the two equations are identical if the appropriate scaling factor is applied. Since the transform variables are of the form $\frac{x}{\lambda f}$ and $\frac{x}{\lambda d}$, respectively, we see that the focal plane distribution is compressed relative to the far-field distribution by the factor $\frac{f}{d}$. For example, the distribution in the focal plane of a 1 m focal length lens is identical in shape but 10^4 times smaller (and more intense) than the distribution 10^4 m from the source.

It is generally more convenient to express the far-field distribution in terms of angle. If we interpret x/d in the far-field as an angle ($\frac{x}{d} = \tan \theta \approx \theta$), the equivalent point in the focal plane distribution is $x_f = f\theta$. Using the 1 m focal length lens as an example again, the field amplitude (U) or irradiance (UU*) occurring at a far-field angle of 1 mrad will occur in the focal plane a distance of 1 mm from the axis. (Consistent normalization is required if absolute rather than relative values are to be obtained.)

3. THE QUESTION OF DEFINITION

Manufacturers' specifications of laser beam characteristics are often vague and inadequate. The problem arises both from inappropriate definitions and from lack of precision in describing the chosen definition.

3.1 Single Transverse Modes

For a laser emitting radiation in certain well characterized modes a single quantity, precisely but somewhat arbitrarily defined, can convey complete information about the beam propagation. Specifically, for a TEM₀₀ (Gaussian) mode given by [5,6]

$$U(x,y) = \frac{2}{\pi} \frac{1}{w} \exp\left[-ik \frac{x^2+y^2}{2R}\right] \exp\left[-\frac{x^2+y^2}{w^2}\right]$$

where $w^2 = w_0^2 [1 + (\lambda z / \pi w_0^2)^2]$

$$R = z [1 + (\pi w_0^2 / \lambda z)^2]$$

and w_0 is the minimum $1/e^2$ (intensity) radius,

it is conventional to define "beam divergence" as that far-field half-cone angle (envelope) inside of which the irradiance is greater than $1/e^2$ of its peak value. This angle is determined from the above equations to be $\lambda / \pi w_0$, and is shown graphically in figure 3-1.

The selection of the $1/e^2$ intensity points is totally arbitrary, but for the Gaussian is convenient. Integration shows that 86% of the energy in the beam is encompassed by that cone angle. Thus simple measurement of fractional energy through a known aperture along with the known wavelength is sufficient to fully characterize the propagation of the beam.

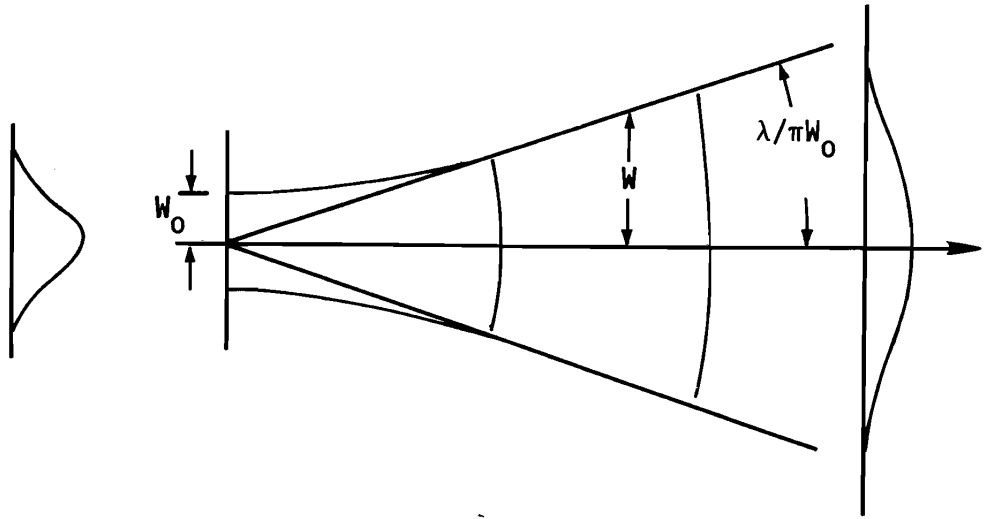


Figure 3-1. Propagation of a Gaussian beam. A single measurement of far-field divergence completely characterizes beam propagation.

Similar techniques [6,7] can in principle be used to characterize higher order modes, for if the mode order TEM_{nm} is known, the propagation laws can be described analytically and related to measurements of energy through an aperture.

3.2 Multimode Beams

Many lasers do not emit in a single transverse mode but rather in a combination of modes often distorted by non-uniform thermal effects. It is for this class of lasers that the specification of beam characteristics by a single parameter becomes difficult if not inappropriate and also for which transformation procedures are most important.

It is common practice with multimode lasers to follow a procedure similar to that for single mode lasers and to specify that half-cone envelope containing some arbitrarily chosen (often 90%) fraction of the energy. This is obtained by placing a series of apertures in the equivalent far-field, the focal plane, and applying the scaling factor given in the previous section. Placement of the aperture is usually for maximum transmission. For sources emitting nominally circular beams with nominally central maxima and for applications where the primary concern is the shape of the beam near the centroid such a procedure may be adequate. A certain precision of definition is required, and we therefore use the notation

$$\theta_{1/2}(f)$$

to denote that half-cone angle containing fraction f of the energy of a single pulse. Later, we will also use the notation

$$\theta_{1/2,x}(f_x)$$

to denote divergence measured in the x - z plane. In this case f_x is defined as though there were no variation of the beam in the y - z plane.

Two principal problems arise with this form of measurement.

1. The output of a Q switched solid-state laser is often grossly asymmetric. It is frequently elliptical and may have multiple maxima, well displaced from the centroid.
2. Both the propagation direction (of, say, the centroid) and/or the profile may vary from pulse to pulse.

If problem 1 is severe, any form of envelope measurements may yield little information of use to the designer, the manufacturer, or the user. In this case it is probable that one should proceed to use a means of obtaining spatially resolved measurements.

If problem 2 is severe, a relatively crude solution is to define an average divergence

$$\theta_{1/2,ave}(f)$$

where the conditions of the average (e.g., first 10 pulses, 50th to 100th pulses, etc.) should be clearly specified.

A greatly superior solution to both problems 1 and 2 is to replace the focal plane aperture with an imaging device such as a videcon, CCD, or detector array, possibly with some additional optics for magnification. This has the advantage of providing information on both complex beam profiles and beam wander. A later section is devoted to a more thorough discussion of these possibilities.

4. SELECTION OF FOCUSING ELEMENT

In choosing a focusing element to provide accurate near-field to far-field transforms and to perhaps satisfy other requirements (e.g., power handling capability) one faces a variety of element types and an infinite selection of parameters. Some guidance can be obtained from optics texts on minimizing aberration. Additional information may be obtained by employing computer-generated spot diagrams. In this section we use the spot diagram method to illustrate the merits of some possible choices.

To use the spot diagram technique we assume that a circular bundle of parallel rays strikes the focusing element at a specified angle. By employing the rules of geometrical optics, each ray is traced through the focusing element to the focal plane and the intersection of each ray with the focal plane is plotted. If this spot diagram is smaller than the spot size calculated to result from diffraction (Airy disc) the performance of the focusing element is expected to approach that of an ideal element. Further calculations (section 5) can then be undertaken to estimate the errors in the transform.

4.1 Refracting Elements

4.1.1 Single Element Lenses

Lens selection involves not only a choice of size and focal length, but also of shape and to some extent index of refraction. We consider here single element thin lenses with spherical or plane surfaces. For such lenses (properly aligned) the principal defect is spherical aberration.

Analysis [8] shows that to minimize spherical aberration in a lens designed to focus nearly collimated light (i.e., an infinite conjugate ratio) a shape factor, q , of $\sim +0.71$ should be chosen ($n=1.5$). The shape factor is defined as

$$q \equiv \frac{r_2 + r_1}{r_2 - r_1}$$

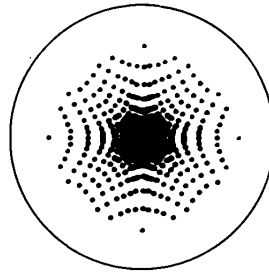
where r_1 and r_2 are the radii of the first and second lens surfaces, respectively. Plano-convex lenses with the plane surface nearer the focus ($q = +1.0$) are sufficiently near the optimum that they are frequently used to meet the condition. This shape factor is also near optimum for minimizing coma, so that such a lens should not be particularly sensitive to alignment.

[It is of great importance that the lens be used with the plane side nearer the focus. A good rule of thumb is that the rays should undergo equal bending at the two surfaces for minimum aberration.]

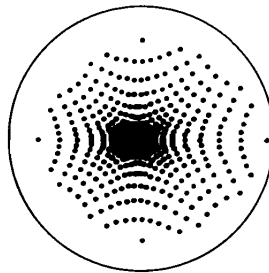
Figure 4-1 shows spot diagrams for an $f/20$ plano-convex lens ($n = 1.5$). In each case the spot diagram is compared with the diffraction limited spot (Airy disc), which for a 10 cm dia aperture at $\lambda = 1.0 \mu\text{m}$ corresponds to a far-field half-angle of 1.2×10^{-5} rad. For on-axis illumination the spot diagram suggests that the lens is essentially diffraction limited. Coma resulting from misalignment is also small for misalignments up to about one degree.

An $f/10$ lens shows significantly more spherical aberration than the $f/20$ lens (figure 4-2(a) compared to figure 4-1(a)) and more coma. A further problem arises from the presence of spherical aberration. The outer zones of the lens focus inside the paraxial focal plane with the result that the location of the minimum spot size depends on how much of the lens is illuminated. For a 1.0 m focal length $f/10$ lens the ambiguity (longitudinal spherical aberration) is about 2 mm, which can be significant (see section 5.4).

From analysis of this type we conclude that at a wavelength of $1.0 \mu\text{m}$ a simple plano-convex lens with an f -number of 20 or greater is a good candidate for transform measurements if reasonable care is taken in alignment. Quantitative assessments of such a choice

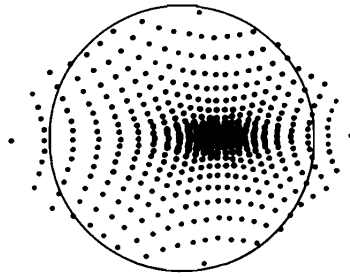


(a)

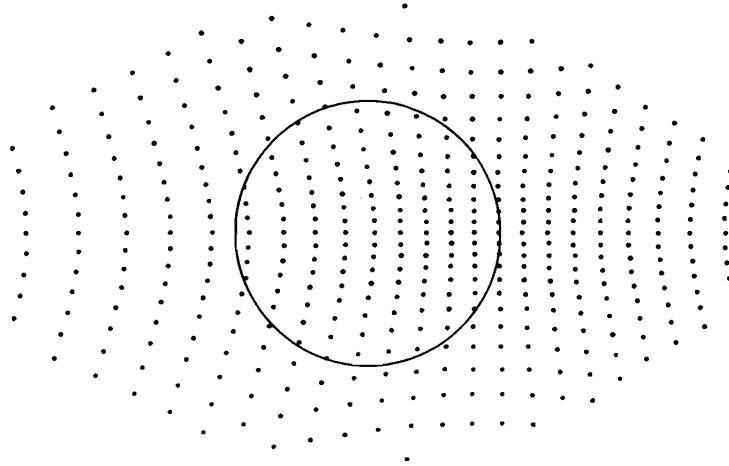


(b)

Figure 4-1. Focal plane and spot diagrams for an f/20 plano-convex lens. Circles represent the diffraction limit (Airy disc) which corresponds to a far-field half-angle of 1.2×10^{-5} rad for a 10 cm dia aperture and wavelength of $1.0 \mu\text{m}$. (a) on axis; (b) 0.5 degree misaligned.

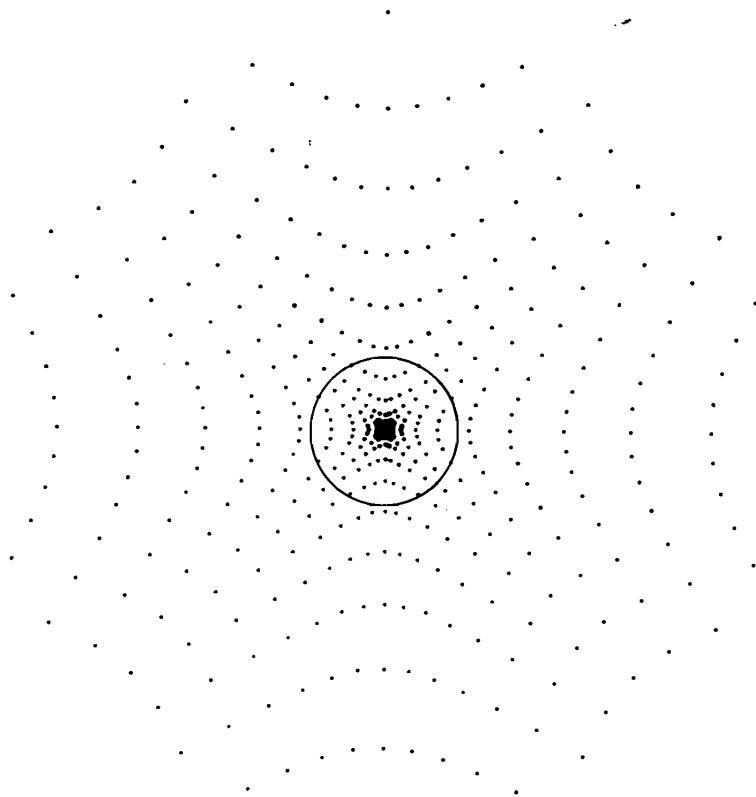


(c)

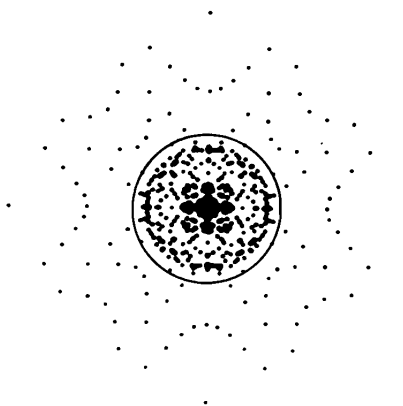


(d)

Figure 4-1. Continued
(c) 1.0 degree misaligned; (d) 2.0 degrees misaligned.

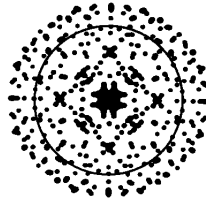


(a)

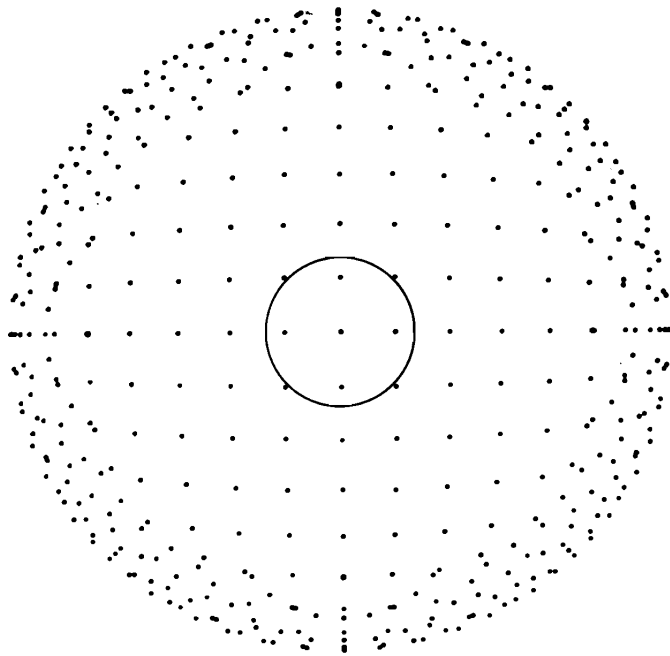


(b)

Figure 4-2. Spot diagrams for an f/10 plano-convex lens. Circles represent the diffraction limit (Airy disc) which corresponds to a far-field half-angle of 1.2×10^{-5} rad for a 10 cm dia aperture and wavelength of $1.0 \mu\text{m}$. (a) at the paraxial focus; (b) 0.9985 f.



(c)



(d)

Figure 4-2. Continued
(c) 0.998 f; (d) 0.9955 f.

will be presented in section 5. At wavelengths shorter than $1.0 \mu\text{m}$, the spot diagram analysis indicates that the $f/20$ lens will cease to be diffraction limited and some other choice should perhaps be made.

4.1.2 Multi-element and Aspheric Lenses

If one wishes to use a low f -number system for transform measurements, more sophisticated lens designs may be utilized. This may also be necessary at short wavelengths. Spherical aberration can be completely eliminated from a single element by correcting the shape (aspherizing). Alternately, both spherical aberration and coma can be greatly reduced by using a two element lens composed entirely of spherical surfaces. No analysis of such systems is presented here because the single element high f -number lens provides the presently required performance and is, as well, more generally available. The techniques employed in this section are, however, directly applicable to more sophisticated systems and could be used to select from various designs.

4.2 Reflecting Elements

In some measurement systems it may be desirable to consider the use of a mirror as the focusing element. A mirror may withstand higher power densities; its focal length is independent of wavelength and may therefore be more easily measurable; and it may result in a more compact measurement system. Mirrors may be analyzed by the same type of geometrical optics approach used for lenses.

4.2.1 Parabolic Mirrors

Among mirrors, the most likely candidate is an off-axis paraboloid, which lacks primary spherical aberration. The geometry of such a system is shown in figure 4-3. By operating off-axis, it is possible to examine the focal plane distribution without disturbing the input beam.

Figures 4-4 and 4-5 show spot diagrams for $f/20$ and $f/10$ paraboloids. For an input parallel to the parabolic axis the spot diagrams consist of a single point (no spherical aberration), but for slight misalignment substantial coma appears. The notation of the figures is that of figure 4-3 with α denoting misalignment in the tangential plane (the plane of the figure) and β denoting misalignment in the saggital plane (perpendicular to the figure). D_{OA} is given in units of the focal length. As before, for a 10 cm dia aperture at $\lambda = 1.0 \mu\text{m}$ the diffraction limit is 1.2×10^{-5} rad.

From figure 4-4 we see that for an $f/20$ reflector a misalignment of 0.5° produces a comatic focal plane spot which is significantly larger than the diffraction limit. For an $f/10$ reflector (figure 4-5) the coma is about a factor of four greater than for an $f/20$ reflector.

Stated in a more useful form, analysis of this type shows that to be diffraction limited an $f/20$ off-axis paraboloid must be aligned to better than about 0.3° (tangential plane) and an $f/10$ paraboloid must be aligned to better than about 0.07° . Alignment in the saggital plane is less critical. Given the greater difficulty of aligning an off-axis reflector compared to a lens (procedures for both cases are discussed in section 6), the above results seem to favor the use of a lens rather than a reflector. Accordingly, the quantitative analysis presented in section 5 assumes the use of a long focal length lens.

4.2.2 Spherical Mirrors

For beam divergence measurements, spherical mirrors must be used off-axis (input not parallel to radius) so that the focal spot is located outside the input beam. This results in substantial aberrations except where very high f -numbers are used. To assess this problem more quantitatively, we have generated spot diagrams for spherical mirrors with various f -numbers and angles of incidence. The results are summarized in the following table.

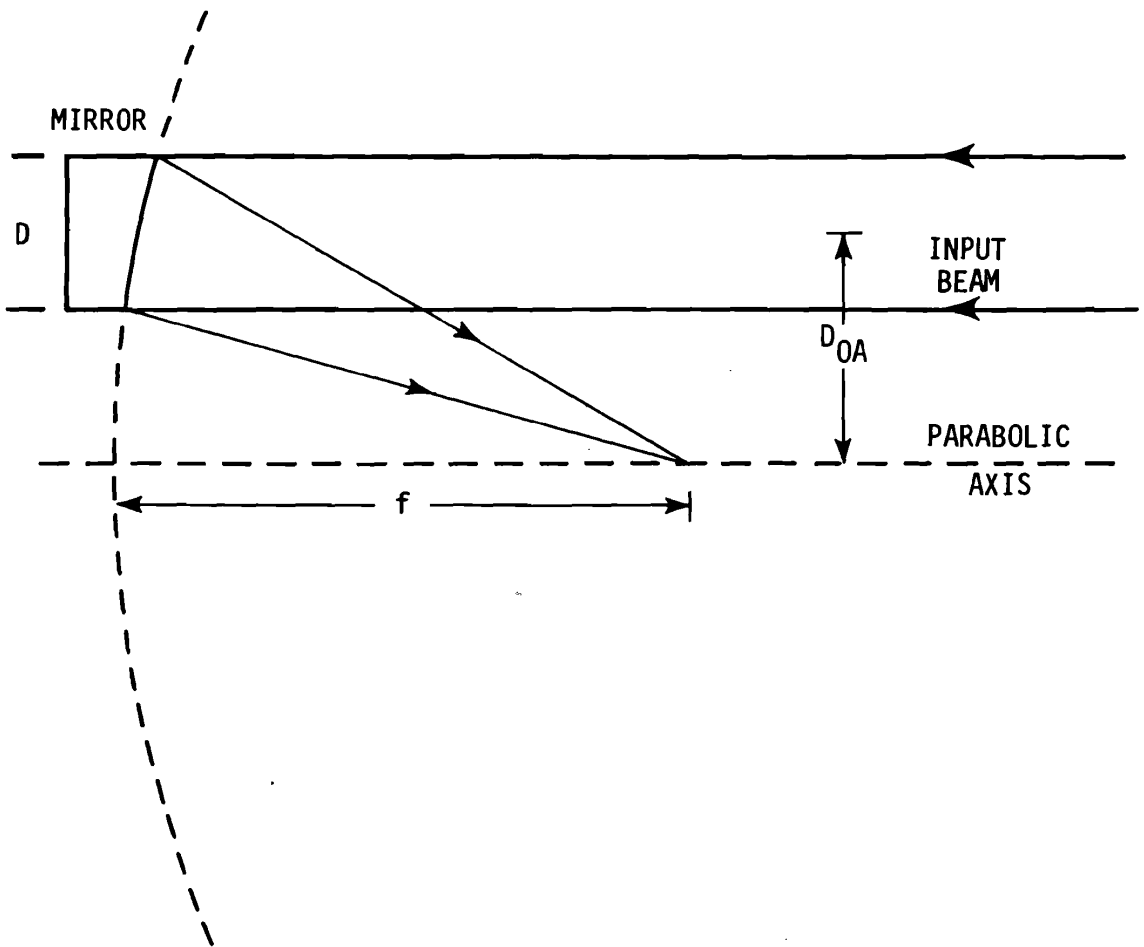
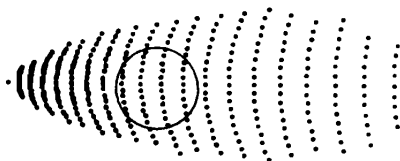
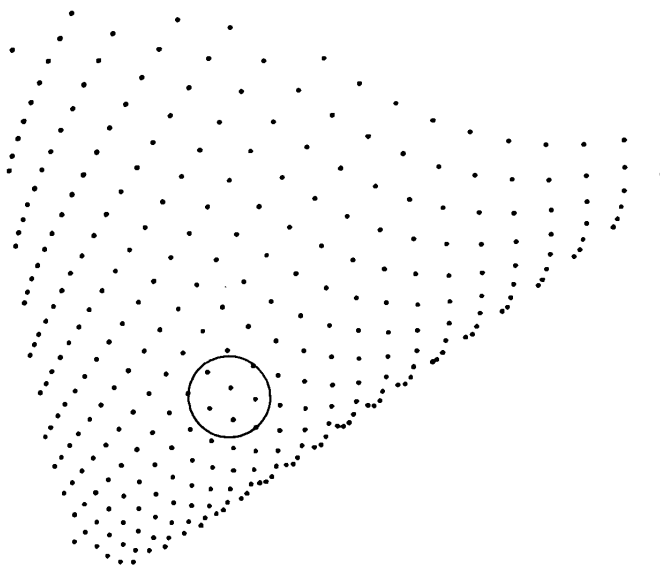


Figure 4-3. The use of an off-axis parabolic mirror for focusing laser radiation.

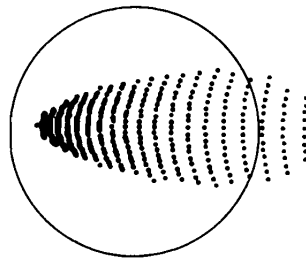


(a)

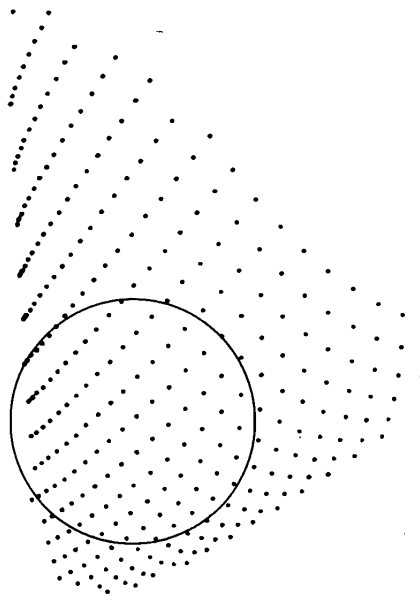


(b)

Figure 4-4. Focal plane spot diagram for an $f/10$ off-axis paraboloid. $D_{0A} = 0.1$; (a) $\alpha = 0.5^\circ$, $\beta = 0.0^\circ$; (b) $\alpha = 0.5^\circ$, $\beta = 2.0^\circ$. Circles represent equivalent far-field half-angles. The diffraction limit for a 10 cm dia lens at $\lambda = 1.0 \mu\text{m}$ corresponds to 1.2×10^{-5} rad.



(a)



(b)

Figure 4-5. Focal plane spot diagrams for an $f/20$ off-axis paraboloid. $D_{0A} = 0.05$; (a) $\alpha = 0.5^\circ$, $\beta = 0.0^\circ$; (b) $\alpha = 0.5^\circ$, $\beta = 2.0^\circ$. Circles represent equivalent far-field half angles. The diffraction limit for a 10 cm dia lens at $\lambda = 1.0 \mu\text{m}$ corresponds to 1.2×10^{-5} rad.

<u>f#</u>	<u>Angle of Incidence</u>	<u>Max Spot Dimension/Focal Length</u>
20	6.0 degrees	5.3×10^{-4}
40	3.0 degrees	6.7×10^{-5}
50	2.4 degrees	3.4×10^{-5}
60	2.0 degrees	1.9×10^{-5}
80	1.5 degrees	8.4×10^{-6}
100	1.2 degrees	4.3×10^{-6}

The angle of incidence is defined as the angle between the direction of beam propagation and the normal to the center of the mirror (radius). Angles listed above are reasonable minimums for each f-number. For a diffraction limited 10 cm diameter beam ($\lambda = 1.0 \mu\text{m}$) the Airy disc diameter divided by the focal length is 2.4×10^{-5} . Thus we expect that those combinations in the above table which yield smaller spot dimensions should be essentially diffraction limited cases for which aberrations are not significant.

5. ESTIMATION OF CERTAIN ERROR SOURCES

5.1 Computational Technique

It would be impossible to provide an error analysis which would incorporate all possible measurement configurations and beam profiles. We therefore resort to the device of attempting to define a typical measurement system and a typical beam profile within the limits of common laser behavior.

Our measurement system is a plano-convex lens, illuminated from the convex side. The diameter is 10 cm and the focal length 200 cm (i.e., an f/20 lens). This choice is based on the analysis of section 4, and the fact that certain systems of interest have apertures this large.

Our "typical" beam profile is chosen more arbitrarily. It consists of a linear combination of several TEM_{nm} modes having the irradiance distribution shown in figure 5-1(a). A wavefront curvature is applied such that the far-field divergence is about $\theta_{1/2,x}(.90) = 1.3 \text{ m rad}$, within the range of 0.1 to 10 m rad typical for systems of interest. Application of wavefront curvature is equivalent in an analytical sense to experimentally defocusing the laser collimator. In addition we also define an "extreme" case. Most of the error sources become more severe when the input beam is larger and when the divergence is smaller. The "extreme" beam is therefore taken to have the same shape as the "typical" beam, but has a larger cross section (figure 5-1(b)) and has a far-field divergence of about 0.13 m rad.

The computations are performed numerically using the approach described in section 1.

1. For the beam under consideration, the far-field distribution is computed.
2. The same distribution is assumed to occur at the input of the lens described above. An appropriate phase factor for the lens is applied along with the appropriate phase factor for propagation to the focal plane. The resulting distribution is then scaled to correspond to the far-field.
3. The irradiance distributions computed from 1 and 2 above are compared to estimate the quantitative error from various sources.

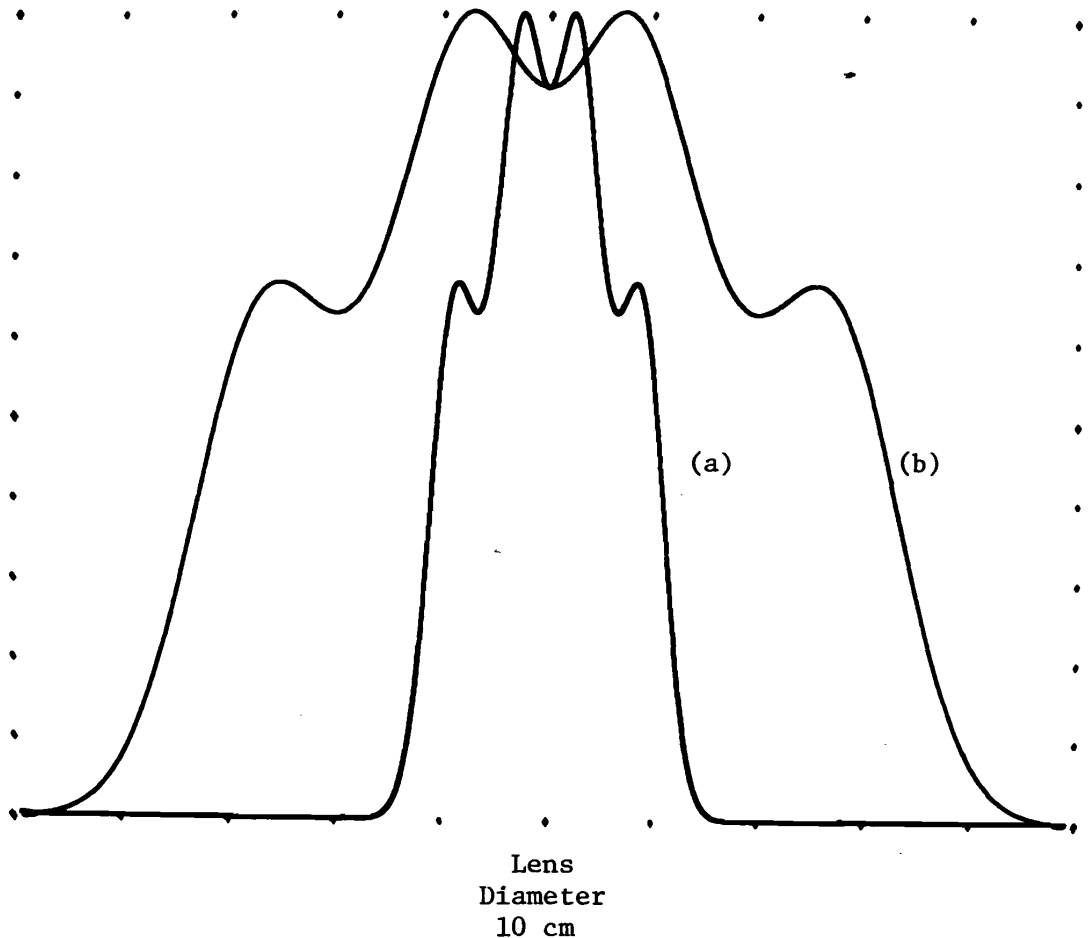


Figure 5-1. Irradiance distributions for two cases examined in this section. In both cases the distribution is formed by a linear combination of TEM_{nm} laser cavity modes. Phase curvature is applied to each case to set the far-field divergence at desired levels. (a) "typical" case, $\theta_{1/2,x}(.9) \approx 1.3$ m rad; (b) "extreme" case, (a) distribution expanded, $\theta_{1/2,x}(.9) \approx 0.13$ m rad.

A fast Fourier transform (FFT) algorithm is used in each of these computations. The primary source of error for this application of the FFT is aliasing due to insufficiently close spatial sampling. This is avoided by application of the sampling theorem, but for the relatively large (in terms of wavelengths) apertures considered here the result is $\sim 10^5$ pieces of data in each dimension ($\sim 10^{10}$ in two dimensions). For low divergence beams fewer samples can be taken, but the volume of data still prohibits routine calculations of this form in two dimensions; we therefore resort to single dimension analysis.

If all functions involved were separable in rectangular coordinates, the above restriction would be of no great consequence. In fact, most beam profiles are not separable at least without approximation. The plane wave propagation factor is separable in the Fresnel approximation as is the phase factor of a lens in the parabolic approximation. When, in the analysis below, extensions from one-dimensional divergence $\theta_{1/2,x}(f_x)$ to two-dimensional $\theta_{1/2}(f_x)$ are made, it should be understood that certain assumptions of symmetry as just outlined are being made. However, even when this symmetry is not present, error estimates thus obtained should be approximately correct.

5.2 The Fresnel Approximation

In section 2.3 we pointed out that in the derivation of the focal-plane/far-field equivalence the Fresnel approximation, though only marginally valid by itself, is largely compensated by the assumption of a non-ideal phase factor for the focusing element. To verify this argument, we can compute numerically, as described above, the focal plane distribution without the Fresnel approximation and with the ideal lens phase factor. We expect this result, properly scaled, to closely coincide with the computed far-field patterns for our test cases. The result for our "extreme" case is shown in figure 5-2. Any difference between the two curves is comparable to or less than the width of the line. We therefore set the following limit to the residual error:

"typical"	"extreme"
$\Delta\theta_{1/2,x}(.9) < 0.1\%$	$\Delta\theta_{1/2,x}(.9) < 0.1\%$

5.3 Lens Aberration

Having shown that the focal-plane/far-field equivalence using an ideal lens is quite good, we now seek to determine the effect of the non-ideal character of our real lens. For our chosen lens we expect spherical aberration to be the dominant defect. Using equation (4.50) of Klein [9] and the additional data that the lens is 1 cm thick and has an index of refraction of 1.5, we compute a distortion to the ideal phase factor of $-3.65 \times 10^{-8} x^4$. The phase factor for our real lens is thus taken to be:

$$\exp -ik[(d^2 + x^2)^{1/2} - d + 3.65 \times 10^{-8} x^4].$$

The resulting error in $\theta_{1/2,x}(f_x)$ depends significantly (in both sign and magnitude) on f_x , the fraction of energy encompassed. This is illustrated in figure 5-3 for our extreme case.

For the two examples used here, we find

"typical"	"extreme"
$\Delta\theta_{1/2,x}(.9) < 0.1\%$	$\Delta\theta_{1/2,x}(.7) = +7.0\%$
	$\Delta\theta_{1/2,x}(.9) = -0.2\%$
	$\Delta\theta_{1/2,x}(.95) = -3.0\%$

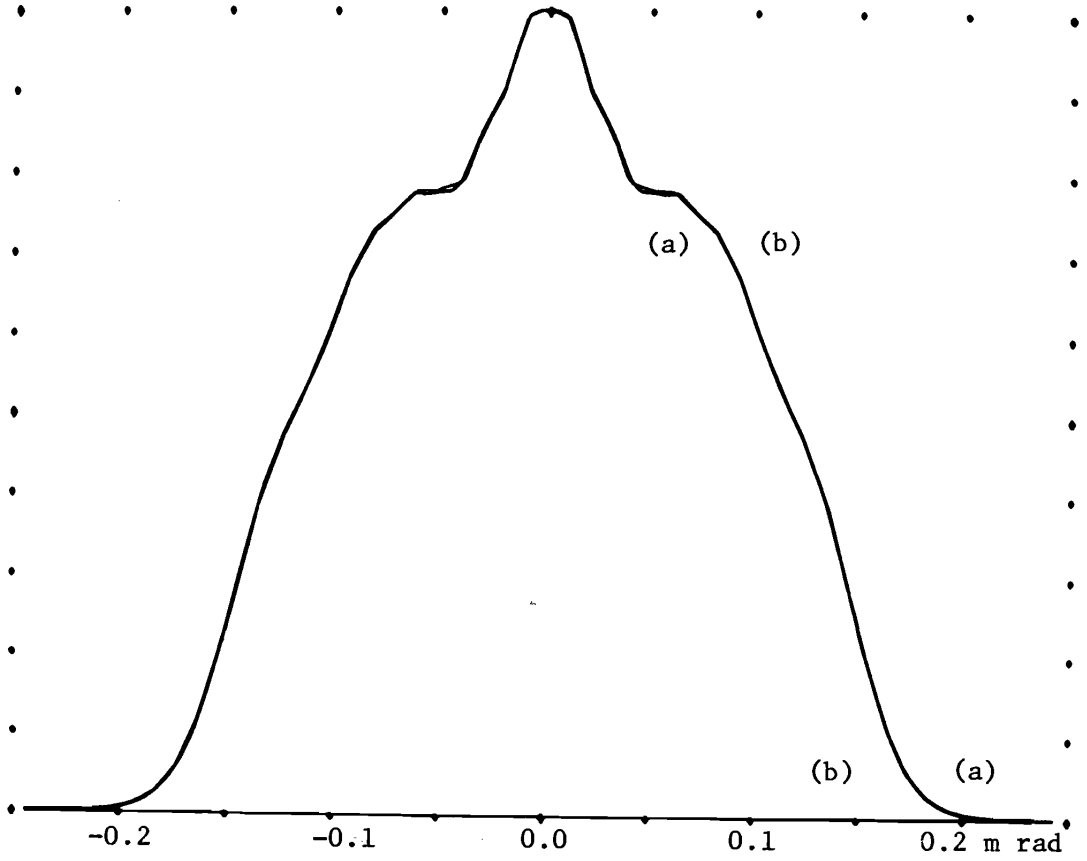


Figure 5-2. Error due to using the Fresnel approximation. The directly computed far-field irradiance pattern for the extreme case is super-imposed upon the scaled focal plane distribution computed without the Fresnel approximation and with the ideal phase factor for a lens.

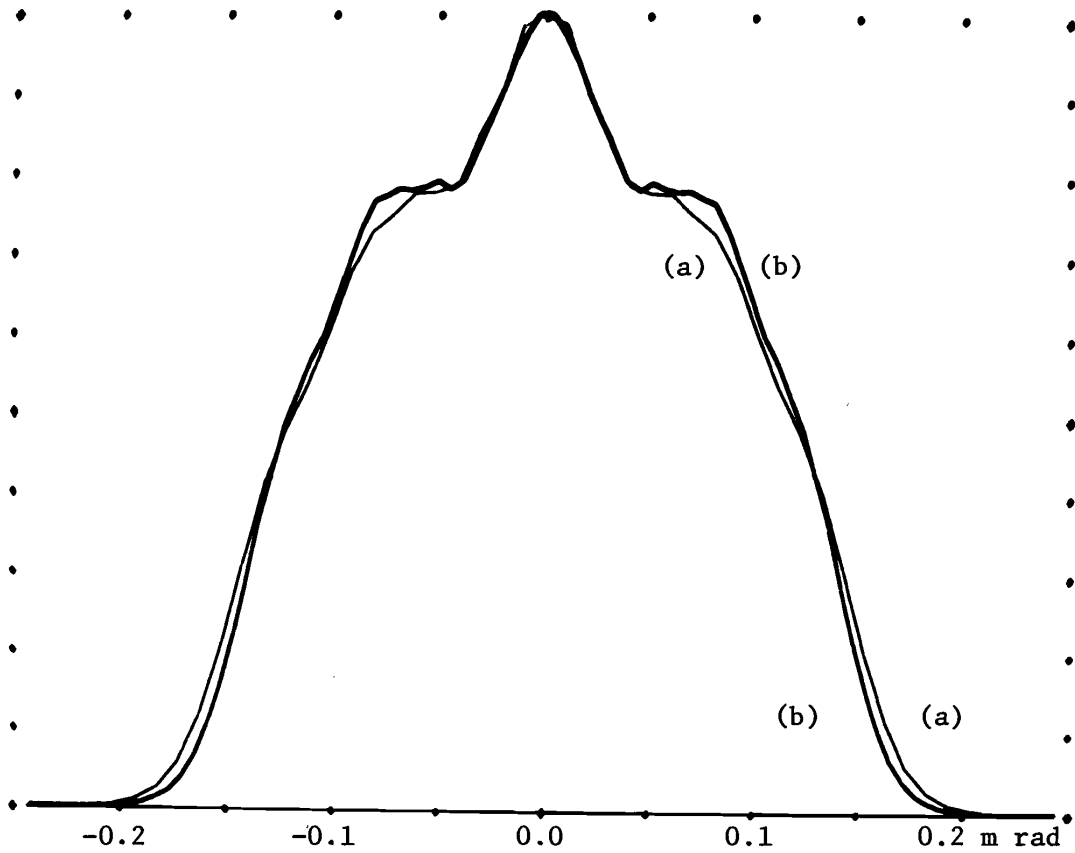


Figure 5-3. Effect of spherical aberration, "extreme" case, $f/20$ lens, 10 cm dia, (a) directly computed far-field distribution; (b) scaled focal plane distribution with spherical aberration present.

The fact that the error is minimum when the fraction of energy encompassed is 0.9 is purely coincidental and a consequence of the beam shape chosen as an example.

We will not treat coma in this section for two reasons. First, we believe that for any reasonable alignment of the lens, spherical aberration should be the dominant aberration. Secondly, the wavefront aberration of coma is not separable in rectangular coordinates, and thus not readily tractable in our one-dimensional analysis. Coma in the tangential plane could be examined, but the results would be of limited usefulness.

5.4 The Position of the Observation Plane

Perhaps the largest quantitative errors result from an improper determination of the focal length and errors in the location of the observation plane. For small errors these effects can be separated.

Since the scaling of the focal plane distribution relative to the far-field is proportional to the focal length, an error in its numerical value propagates directly in one dimension. Thus, for a 1% error in determination

$$\Delta\theta_{1/2,x}(.9) = 1\%.$$

Appropriate means for establishing the numeric value of the focal length will be discussed in section 6.

The error resulting from improper placement of the observation depends critically on the magnitude of the divergence. For the case of a slightly defocused laser beam such as we have been using for test purposes this fact is illustrated in figure 5-4. Specific calculations yield the following results:

1% misplacement (2 cm)

"typical"

$$\Delta\theta_{1/2,x}(.9) = \pm 1.7\%$$

"extreme"

$$\Delta\theta_{1/2,x}(.9) = \pm \text{factor of 5}$$

0.05% misplacement (0.1 cm)

"typical"

$$\Delta\theta_{1/2,x}(.9) < 0.1\%$$

"extreme"

$$\Delta\theta_{1/2,x}(.9) = \pm 6.6\%$$

Figure 5-5 shows irradiance computations for the extreme case.

These results point out the great importance of determining the focal plane properly and properly placing the observation device. In the infrared, these tasks are more difficult than in the visible. Further discussion of proper procedures is contained in section 6.

It should also be noted that for beams with relatively low divergence it is possible to under estimate very substantially the divergence by placing the observation device too far from the lens.

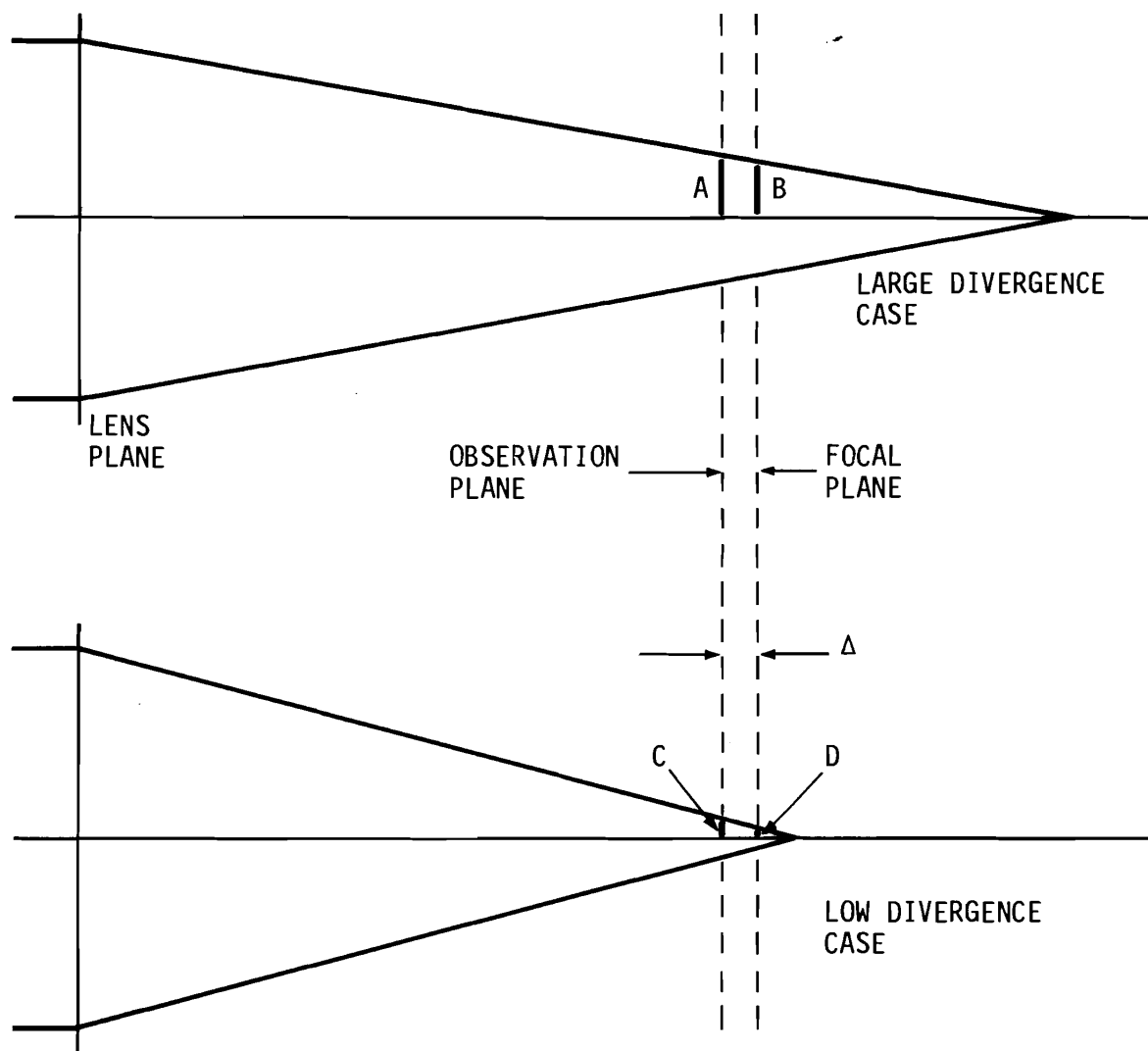


Figure 5-4. Effect of incorrectly placed observation plane in the geometrical approximation. For the same error, Δ , in the placement of the observation plane, the error in spot size becomes much greater for low divergence beams. That is $\frac{C}{D} \gg \frac{A}{B}$.

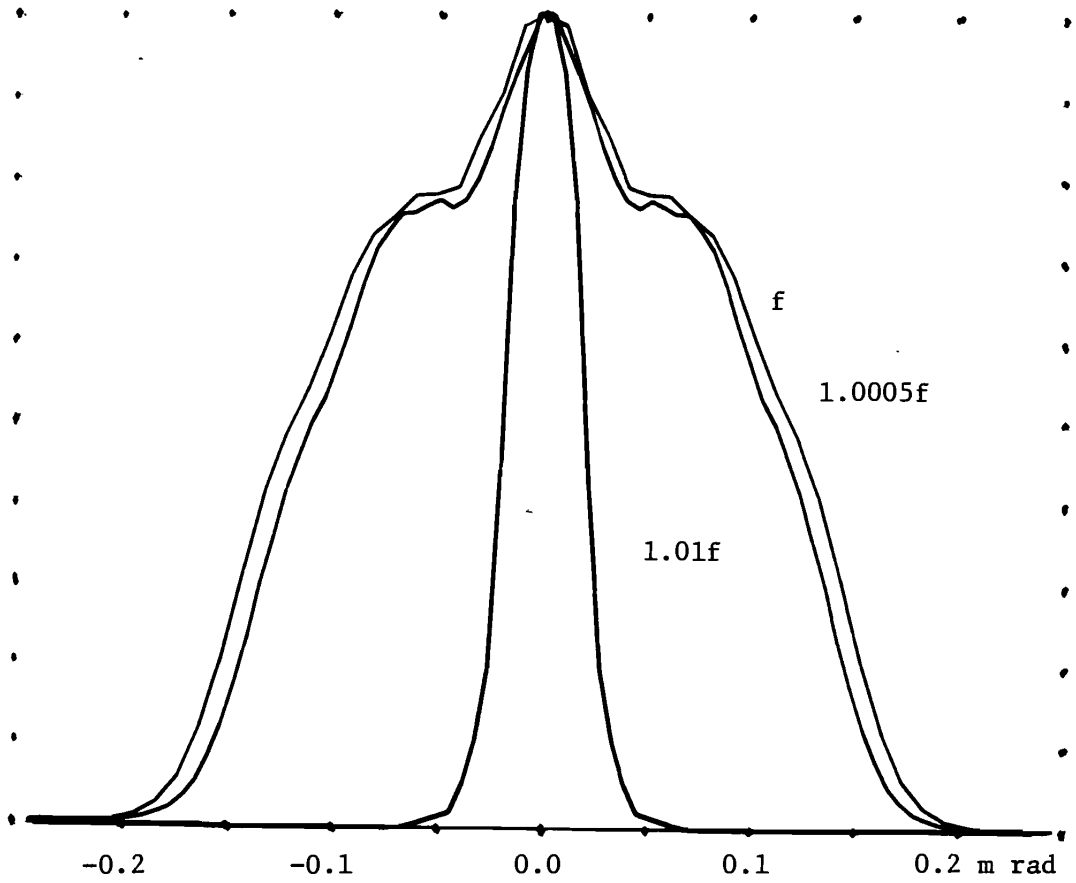


Figure 5-5. Effect of misplacement of observation plane.
"Extreme case."

5.5 Summary of Computations

The results of computations in this section are tabulated as follows:

<u>Errors in $\Delta\theta_{1/2,x}(f_x)$</u>				
($f_x = 0.9$ unless specified)				
<u>Source</u>	<u>"typical"</u>		<u>"extreme"</u>	
Fresnel Approximation	< 0.1%		< 1%	
Spherical Aberration	< 0.1%		(0.7) + 7.0%	(0.9) - 0.2%
			(0.95) - 3.0%	
Observation Plane Location:	$\Delta = \pm 1\%$	$\Delta = \pm 0.05\%$	$\Delta = \pm 1\%$	$\Delta = \pm 0.05\%$
Scale factor	$\pm 1\%$	$\pm 0.05\%$	$\pm 1\%$	$\pm 0.05\%$
Location	$\pm 1.7\%$	< 0.01%	$\pm X5$	$\pm 6.6\%$

It is important to remember the difference between the definitions of $\theta_{1/2}(f)$ and $\theta_{1/2,x}(f_x)$. The former is defined as a cone angle (a plane angle of revolution) while $\theta_{1/2,x}(f_x)$ is defined from the profile cross section in the x-z plane only. For beams which are generally circular, $\theta_{1/2}(f)$ and $\theta_{1/2,x}(f_x)$ are comparable [Ex: Gaussian beam - $\theta_{1/2}(.86) = \frac{\lambda}{\pi\omega_0}$, $\theta_{1/2,x}(.86) = 1.045 \frac{\lambda}{\pi\omega_0}$] and therefore $\Delta\theta_{1/2}(f) \approx \Delta\theta_{1/2,x}(f)$. If, instead, the beam is substantially elongated in one dimension, $\theta_{1/2}(f)$ approaches the one dimensional value for the larger dimension.

Any generalization of the error sources in a measurement process into a single estimate of uncertainty is hazardous. This is particularly true when, as in this case, the contributions of each error source depend, often critically, on the details of the source to be measured. The philosophy of this analysis has, therefore, been to examine specific cases and to observe the error contributions and their sensitivity to the parameters of the measurement system and to some of the parameters of the source. The extent to which these chosen cases are typical or worst cases cannot be established. If we nevertheless assume that what we have called a "typical" case is representative of 1 μm wavelength beams of several centimeters diameter and nominal divergence of 1 m rad, the above analysis suggests that measurements of $\theta_{1/2}(.9)$ to uncertainties of 2-3% should be possible with reasonable care. Further, if our "extreme" case is, in fact, typical of sources nearly filling a 10 cm diameter aperture and having nominal divergence of 0.1 m rad, the above analysis suggests that very careful attention to detail may be necessary to achieve uncertainties of less than 10%.

Some improvement in accuracy may be obtainable by employing a lens which is corrected for spherical aberration, though in most cases this will not be worth the additional cost. The principal source of error will likely remain the positioning of the observation plane.

6. EXPERIMENTAL IMPLEMENTATION

6.1 Characterizing the Focusing Element

We turn now to measurements and tests on the focusing element which must be made prior to use. Of critical importance is the numeric value of the focal length and the position of the focal plane at the wavelength of interest. In addition, it is desirable to check for unexpected aberrations and to appropriately align the element with the optical bench or test facility to be used. Many techniques for these purposes can be found in the literature. In this section we describe some of the more simple tests and their adaptation to present needs.

6.1.1 Lenses

When accurately specifying the focal length of a lens it is usually necessary to use thick lens terminology. For a more complete discussion of this terminology see chapter 5 of reference [8].

The focal length of a lens is properly measured from the secondary principal plane of the lens, which is defined in a geometrical optics sense as the plane of intersections between parallel input rays (extended) and the bundle of rays (extended) which converge to the focal point (figure 6.1). This "focal length" is to be distinguished from the "back focal length" which is measured from the back surface of the lens.

When the index of refraction on each side of the lens is the same, the secondary principal plane contains the secondary nodal point (figure 6.1). The secondary nodal point has the useful property that when the lens is rotated through small angles about it as center the focus does not move laterally. This forms the basis for the nodal slide technique of focal length determination.

The nodal slide is simply a device which allows the lens to be rotated about any point on its axis. It can be used in conjunction with a high quality collimator (figure 6.2(a)) or more simply in auto-collimation (figure 6.2(b)). In the latter case a source at the appropriate wavelength (perhaps a cw laser) is focused through a pinhole. Using the test lens and a high quality flat mirror as shown, the image of the pinhole is located along side the pinhole (as close as reasonably possible). By successive translation and rotation an axis of rotation is found which results in no lateral movement of the image. This axis contains the secondary nodal point and the focal length is measured from this axis to the pinhole.

As one check on this procedure, the location of the secondary principal plane can be computed knowing the shape and index of refraction of the lens. The procedure is given in reference [8], chapter 5. For a 2 m focal length lens ($R_1 = 1$ m, $R_2 = \infty$, $n = 1.5$, thickness = 1 cm) the secondary principal plane is found to lie inside the lens 6.7 mm from the plane surface.

The nodal slide also provides a means of aligning the lens with the optical bench. With the lens center and the pinhole both centered on the bench, and the same distance above it, the lens can be rotated a few degrees in each direction until a small amount of coma appears in the image. By symmetry the best orientation of the lens can be determined. Using this method it is convenient to align the lens described in the previous paragraph to better than one degree.

A second, complementary, approach to evaluating a lens is the use of wave-front shearing interferometry. This technique provides a convenient cross-check of focal length measurements made with a nodal slide. It also provides information about aberrations present in the system. The setup for this measurement is shown in figure 6.3. As with the nodal slide, a pinhole source is placed near the focal plane of the test lens. A shearing plate, typically a piece of high quality optical glass or other transparent material having

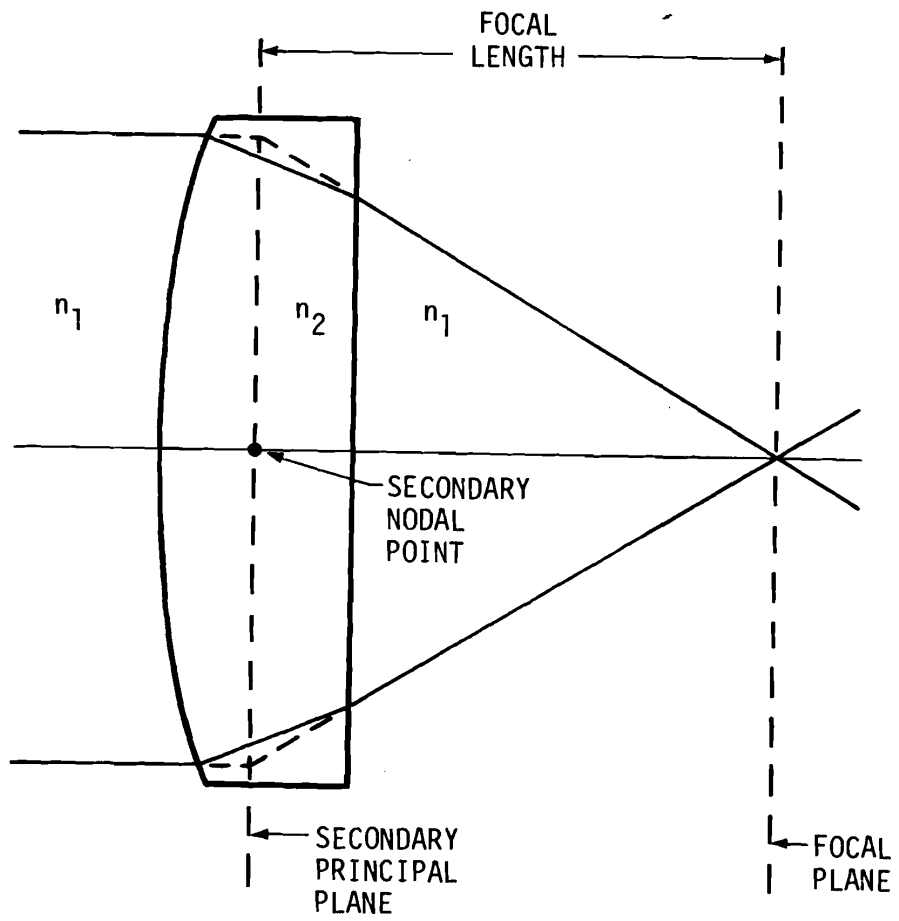
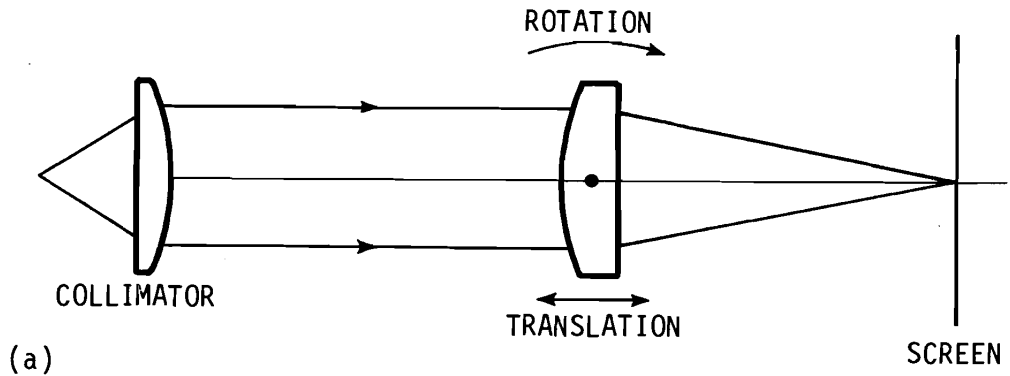
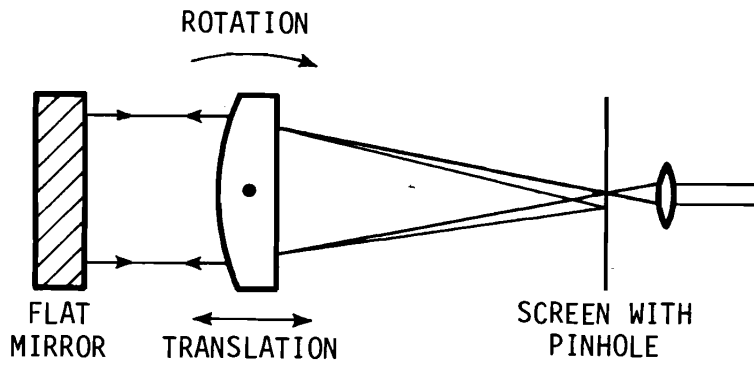


Figure 6-1. Parameters of a thick lens.



(a)



(b)

Figure 6-2. The use of a nodal slide to determine the focal length of a lens. (a) Using a collimated source; (b) in autocollimation.

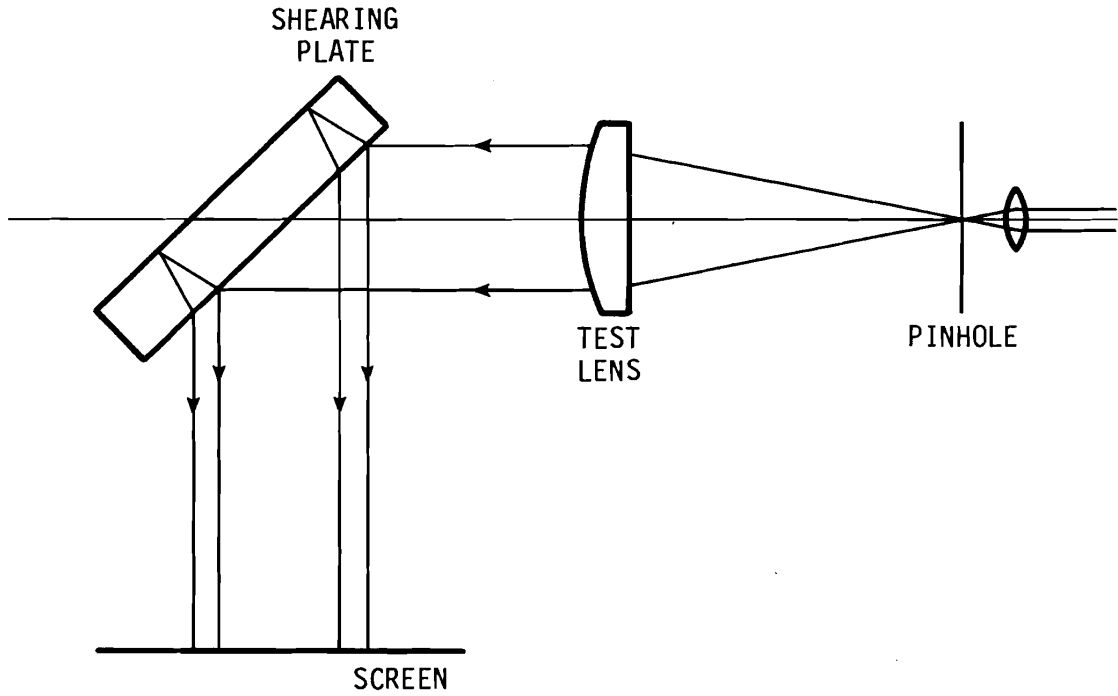


Figure 6-3. The use of a wavefront shearing plate to determine the focal length of a lens.

flat and nearly parallel faces, is placed in the collimated beam at an angle to the direction of propagation. Interference fringes are produced on a screen by the reflections from the front and back faces.

If the pinhole is not in the focal plane of the lens the interference pattern is that of two offset spherical waves, and consists of linear fringes. As the radius of the spherical wavefronts increases (the pinhole is moved closer to the focal plane) the spacing of the fringes increases. For plane wavefronts (pinhole in focal plane) and exactly parallel faces on the shearing plate the fringe spacing becomes large compared to the beam diameter.

Increased precision can be obtained by polishing the faces of the shearing plate with a slight wedge. If the apex of the wedge is parallel to the shearing plane (the plane of the paper in figure 6.3) the fringe spacing does not approach infinity as the pinhole is passed through the focal plane, but reaches a limit determined by the wedge angle, while the orientation rotates through 180°. For plane wavefronts, the fringes are parallel to the shearing plane.

This is illustrated in figure 6.4 which shows computer simulated fringes for a 2 m focal length plane convex lens at 632.8 μm . When the pinhole is at the focal plane, the fringes at the center of the interference pattern are seen to be parallel to the shearing plane, while spherical aberration causes slight curvature to the fringes at the edge. Since the fringe separation corresponds to one wavelength of phase deviation, we see that the maximum phase error is about $\lambda/5$.

Figure 6.5 shows the experimental equivalent of figure 6.4. Comparison of the two figures suggests that the lens used is slightly corrected for spherical aberration. Both figures indicate that a precision of $\pm 1 \text{ mm}$ ($\pm .05\%$) in determining the focal length of such a lens is possible by this technique. It should be noted, however, that it is the focal plane which is found in this manner, and computation (as indicated previously) is required to get the actual focal length.

The computed and experimental patterns of figures 6.4 and 6.5 were produced at a wavelength of 0.63 μm for ease of illustration. At a wavelength near 1 μm the same results will hold, except that the fringe spacing will be proportionately larger and the phase error proportionately smaller.

To conclude this discussion on lens evaluation we present below a summary of data on a single lens of the type described in this and previous sections.

<u>Method</u>	<u>Focal length</u>		
	$\lambda = .63\mu\text{m}$	$\lambda = 1.06\mu\text{m}$	$f_{1.06}/f_{.63}$
Nodal slide	198.84 cm	202.19 cm	1.0168
Wavefront shearing	198.93 cm	202.19 cm	1.0164

Based on dispersion data for the glass (BK7) used in the lens we expect the ratio of focal lengths to be 1.0167. These results further suggest that, with a small loss in confidence one may perform the focal length determination at some known, available source wavelength and extrapolate from dispersion data to the desired wavelength.

6.1.2 Mirrors

One advantage of using reflective elements, especially for infrared systems, is that they can be characterized at any convenient wavelength. In the case of the off-axis paraboloid, this is offset significantly by the problem of locating the parabolic axis.

For the paraboloid, a simple approach is to use a wavefront shearing plate as shown in figure 6.6(a). The mirror is moved relative to the pinhole until the interference pattern consists of straight lines parallel to the shearing plane. At this point, the pinhole is located at the focal point on the parabolic axis and the collimated beam is parallel to the

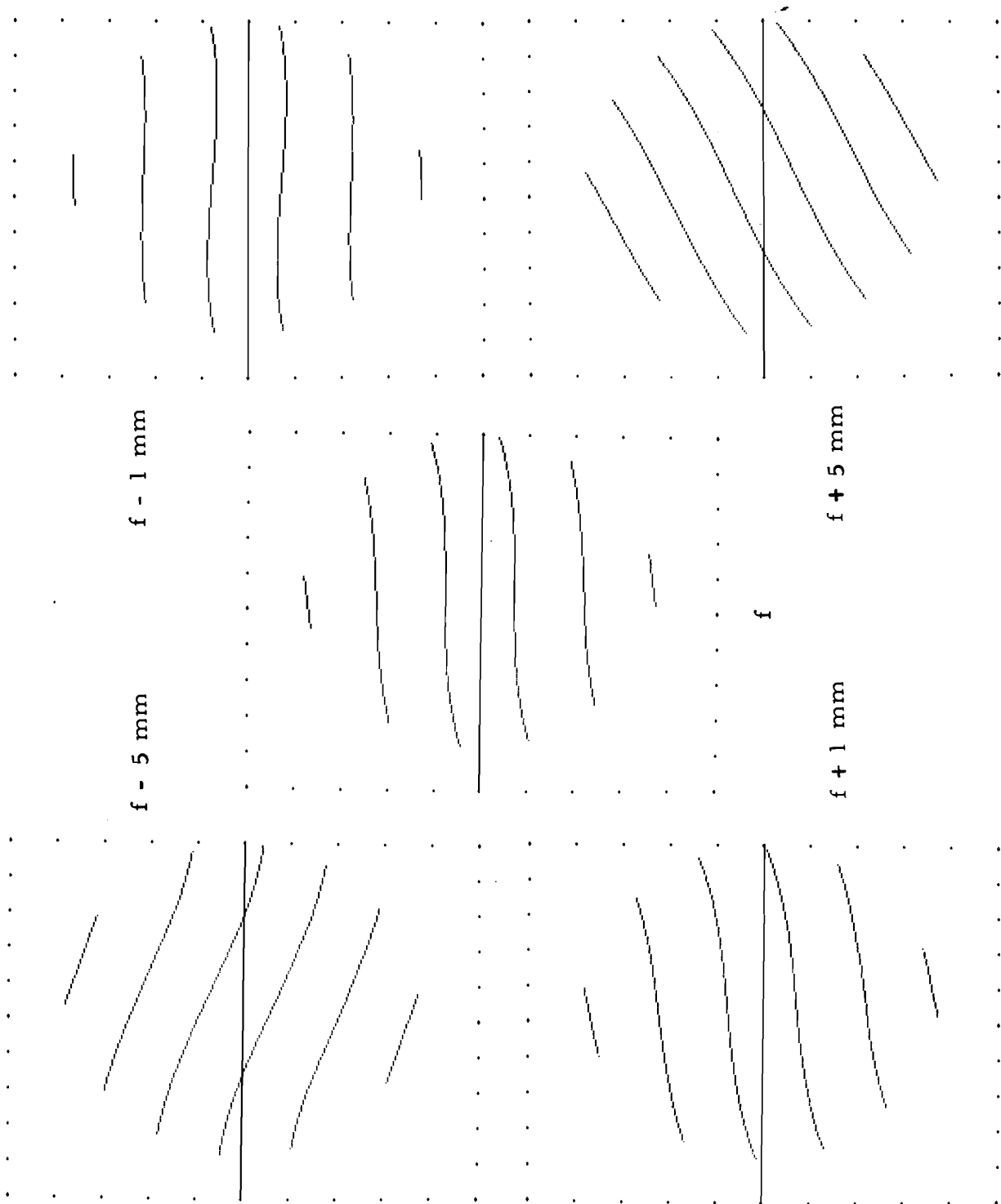
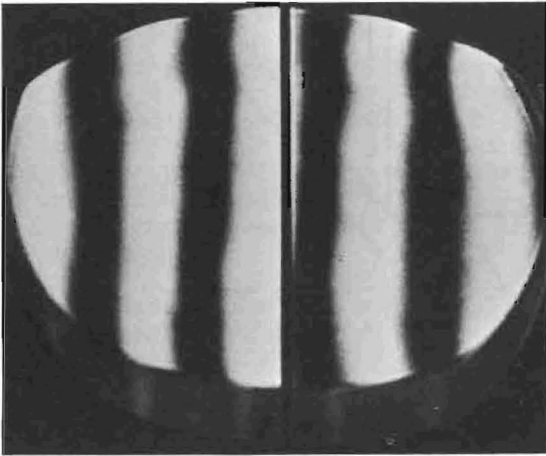
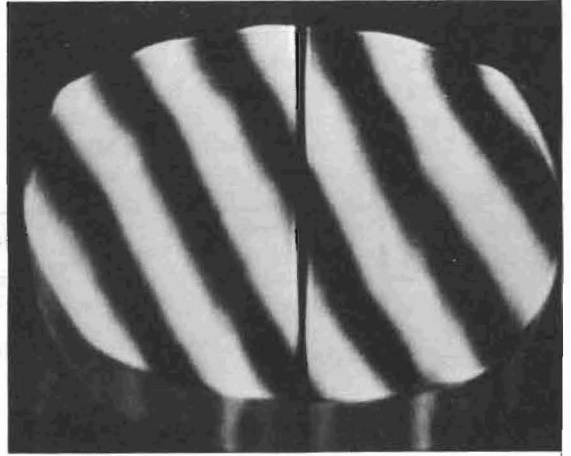


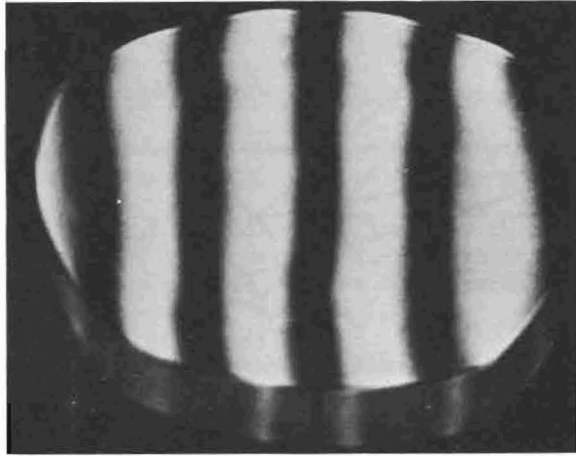
Figure 6-4. Computed simulated fringe patterns for the arrangements shown in figure 6-3. Individual patterns are for the indicated distances between lens and pin-hole. The program assumes $\lambda = .63 \mu\text{m}$ and $f = 200 \text{ cm}$. The two reflected beams are offset by 1.2 cm and propagate in directions differing by $3.3 \times 10^{-5} \text{ rad}$.



$f - 1 \text{ mm}$



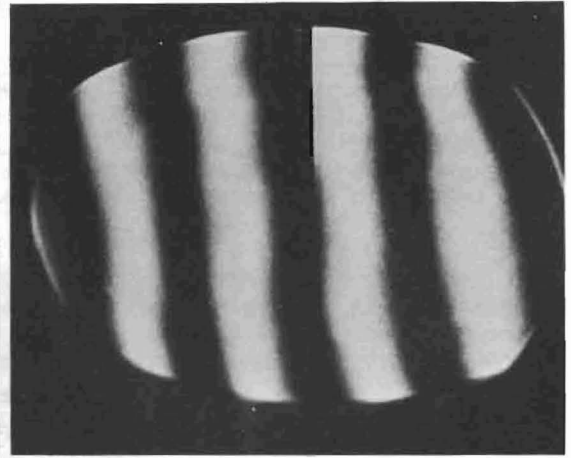
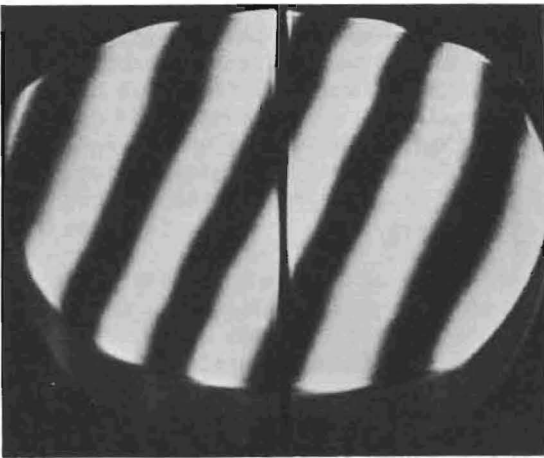
$f + 5 \text{ mm}$



f

$f - 5 \text{ mm}$

$f + 1 \text{ mm}$



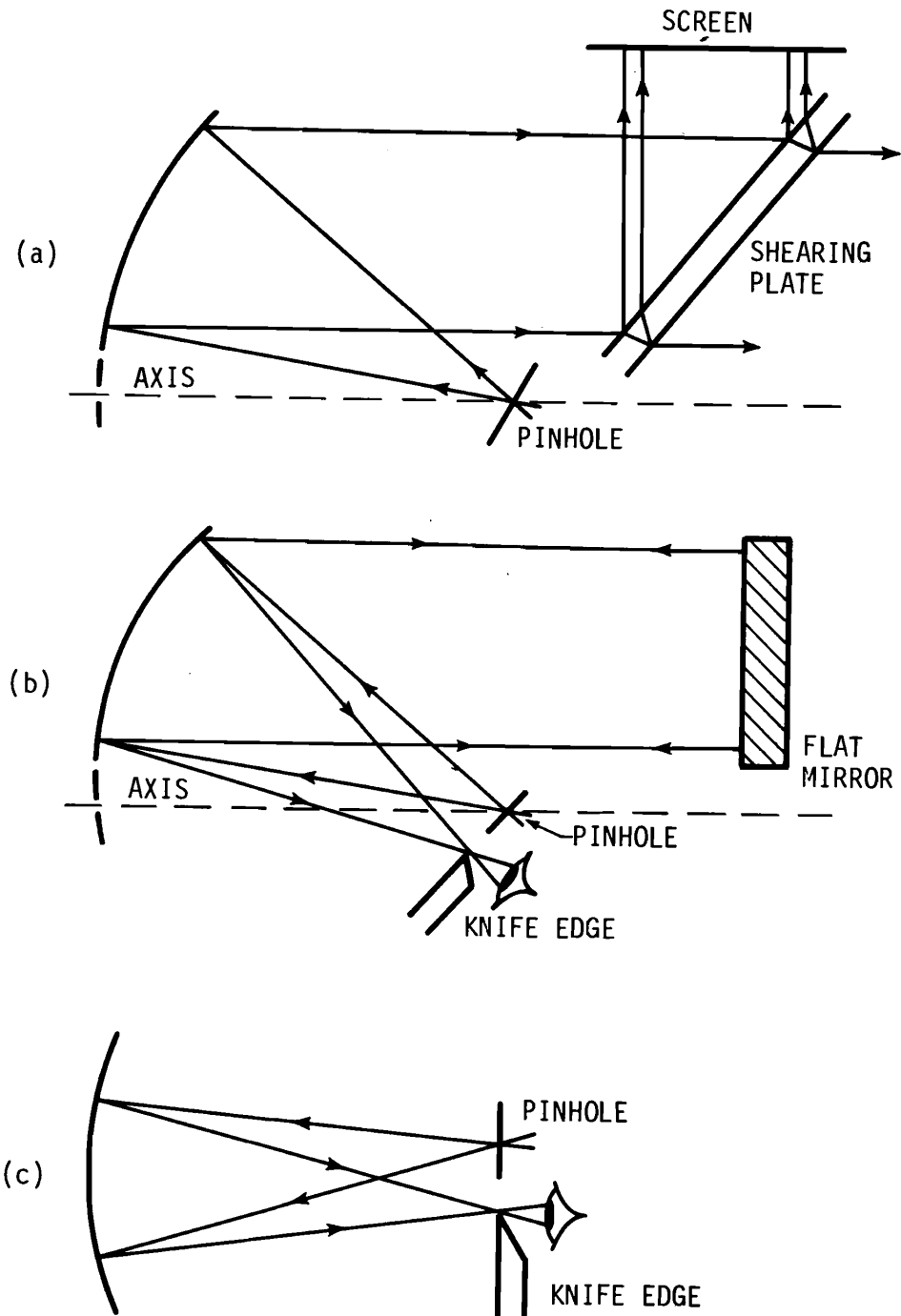


Figure 6-6. Techniques for determining the focal length of a mirror. (a) A shearing plate used with a parabolic mirror; (b) the knife edge technique for a parabolic mirror; (c) the knife edge technique for a spherical mirror.

axis. As with a lens, residual curvature in the fringes is a measure of the aberrations introduced by the mirror.

It should be possible to use this same technique to examine a spherical mirror. In this case the least aberration is obtained as near the collimated beam as possible.

As an alternate means of determining the focal length of a mirror, one can employ the Foucault (knife edge) test. This is illustrated for a parabolic mirror in figure 6.6(b). The apparatus consists of a pinhole which is co-planar with a moveable knife edge. If the pinhole is located in the focal plane, the observer will see the mirror darken suddenly and uniformly as the knife edge is passed through the image of the pinhole. If the pinhole is located in front or in back of the focal plane, the image will not lie in the plane of the knife edge. Consequently, when scanning, the observer will see the mirror darken gradually and non-uniformly.

Imperfections in the lens can be thought of as regions of different focal length. Thus the uniformity with which the mirror darkens is a measure of mirror quality. Simple geometric optics suggests that for a 200 cm focal length mirror, deviations in the mirror of the order of 0.1 μm can be detected.

The Foucault test can also be applied to spherical mirrors, either in a manner like that of figure 6.6(b) or by placing the pinhole and knife edge at the center of curvature (figure 6.6(c)). This is possible because the image of an object at the center also lies at the center of curvature.

6.2 Other Experimental Considerations

In this section we wish to point out some experimental problems which may arise in performing envelope divergence measurements. Typical setups are indicated in figure 6.7.

The laser under test must first be aligned collinear with the optic axis of the system as defined by the lens/mirror axis, the aperture, and the optical bench. Procedures for performing this will depend greatly on the type and characteristics of the laser under test and are therefore not discussed further here.

It is desirable that the focusing element be placed as far as possible from the laser to minimize the collection of scattered light and (if the light is unfiltered) of light from the pumping source. In the case of the lens, this will also help minimize feedback into the laser. (A high efficiency anti-reflection coating on the lens should also be employed for this purpose if expected power densities will allow it.)

In selecting apertures, size and damage resistance are important considerations. The required determination of aperture dimensions is generally within the capability of a machine shop although for small apertures some uncertainty may be introduced. An inaccuracy of 0.001 inch in the diameter of a 1 mm aperture results in an inaccuracy in area of 5%. Optical damage at the edge of the aperture may result in the emission of radiation (which will be detected along with laser radiation) as well as dimensional changes. If levels high enough to produce damage are expected, it is well to use apertures of a reflective or damage resistant material.

Since the data of interest is the ratio of power/energy transmitted through a known aperture to the total power/energy, calibration accuracy of the monitor is of little concern as is linearity since the quantities typically differ by only 10-20%. Other factors affecting precision, for example, spatial uniformity of response, are of much greater importance in selecting an instrument.

In many cases the reproducibility of the laser, in amplitude, in profile, and in direction of propagation, will set the limit to measurement quality. Variations in amplitude can be compensated by the use of a beamsplitter and monitor (figure 6.7). Several difficulties arise with this approach:

- (1) The beamsplitter must be wedged to avoid interference effects; this deviates the beam and makes alignment difficult.

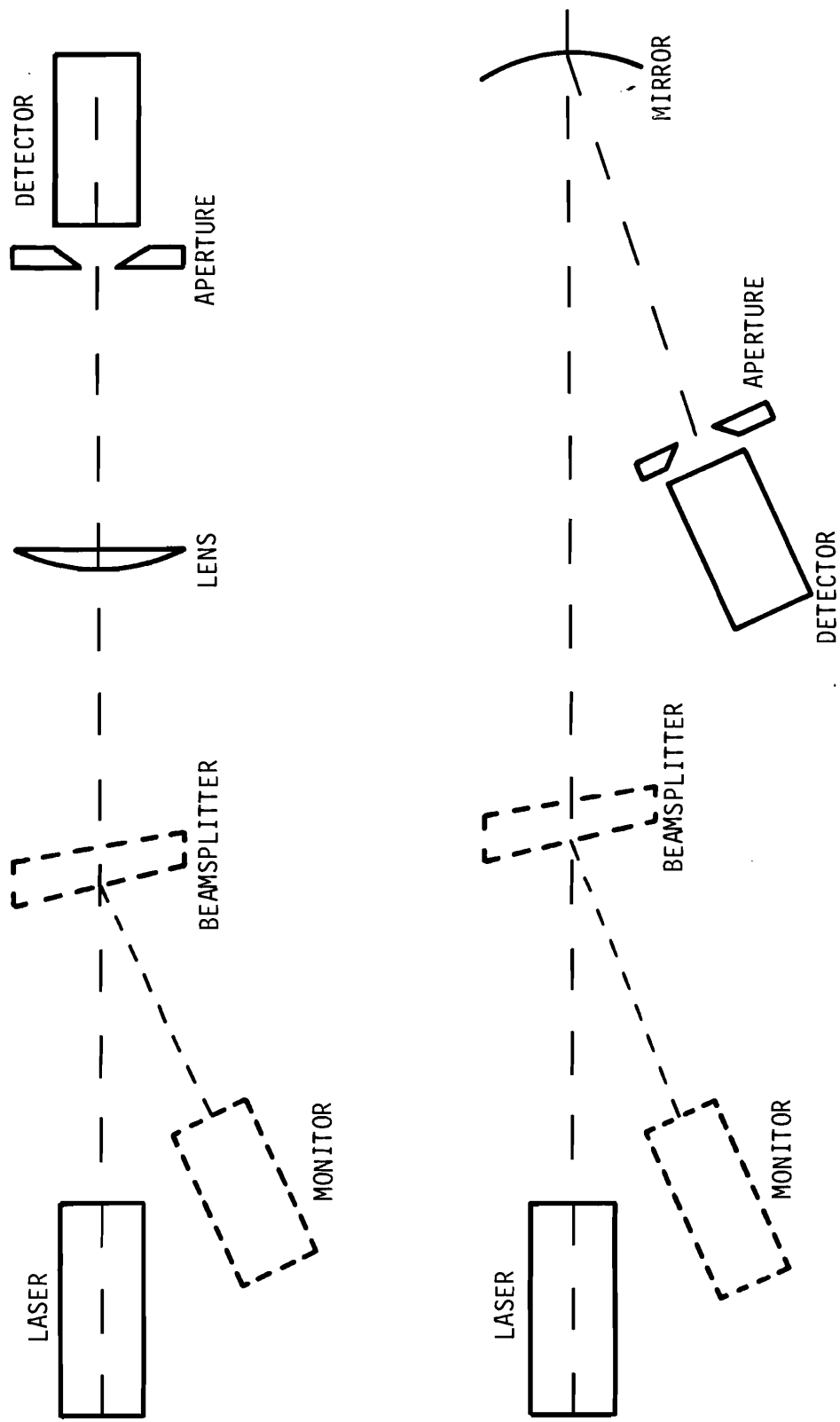


Figure 6-7. Typical setups for using a lens or a mirror to measure laser far-field beam divergence.

- (2) The reflection coefficient is polarization sensitive; if the laser is randomly polarized and the angle of incidence is more than a few degrees, the ratio of transmission to reflection will show significant scatter.
- (3) The beamsplitter may modify the transmitted beam through phase distortion or multiple reflections.

Variations in beam deviation can be examined to some degree by mounting the aperture on a translation stage allowing motion perpendicular to the system axis.

Variations in profile from pulse to pulse are not usefully examined with envelope measurements. Some possible approaches to this problem are discussed in the next section.

7. SPATIALLY RESOLVED MEASUREMENTS

In the preceding sections we have indicated the deficiencies of envelope divergence measurements for complex beam profiles and where variations with time occur. An obvious question is whether detailed beam profiles can be obtained with good resolution and accuracy from the focal plane transform measurement system. Beyond the approximations of the transform discussed in this document, the answer rests with the technology of imaging devices.

For beams exhibiting no time dependence, scanning a small detector across the focal plane distribution may yield sufficient spatial information. In general, however, an array or imaging device might be placed in the focal plane or in an equivalent image plane to provide magnification (figure 7-1). Introduction of additional optics should not necessarily add additional inaccuracy because, as in a telescope, the quality of the transform lens (objective) will normally have the dominant effect on image quality.

A suitable image device should be linear over 2 to 3 decades of irradiance and be simultaneously uniform over its surface. Resolution requirements will depend on the particular application but even as few as 10 elements across a typical beam diameter would provide substantial improvement over envelope measurements. A suitable storage mechanism must be employed to observe waveforms of pulsed sources. Exploratory work must be performed to determine whether the above conditions can be met and the extent to which the quality of the imaging device will effect the complete measurement process.

In the visible and near infrared portions of the spectrum, the most likely candidates will be among tubes designed for television-type applications. Conventional vidicons do not, in general, provide either sufficient linearity or uniformity; however, silicon diode array tubes do show apparently sufficient linearity and may be sufficiently uniform at wavelengths significantly shorter than the band gap [10]. CCD vidicons may provide still better linearity and uniformity but at some loss in resolution with present commercial tubes. A wide variety of image processing hardware (readout, storage, analog and digital processing) is commercially available to be used with such tubes thus making automated measurement techniques immediately feasible.

At longer wavelengths the choices are less clear. Some image tubes are presently available but less is known about their performance capabilities. Arrays of individual detectors should also be considered.

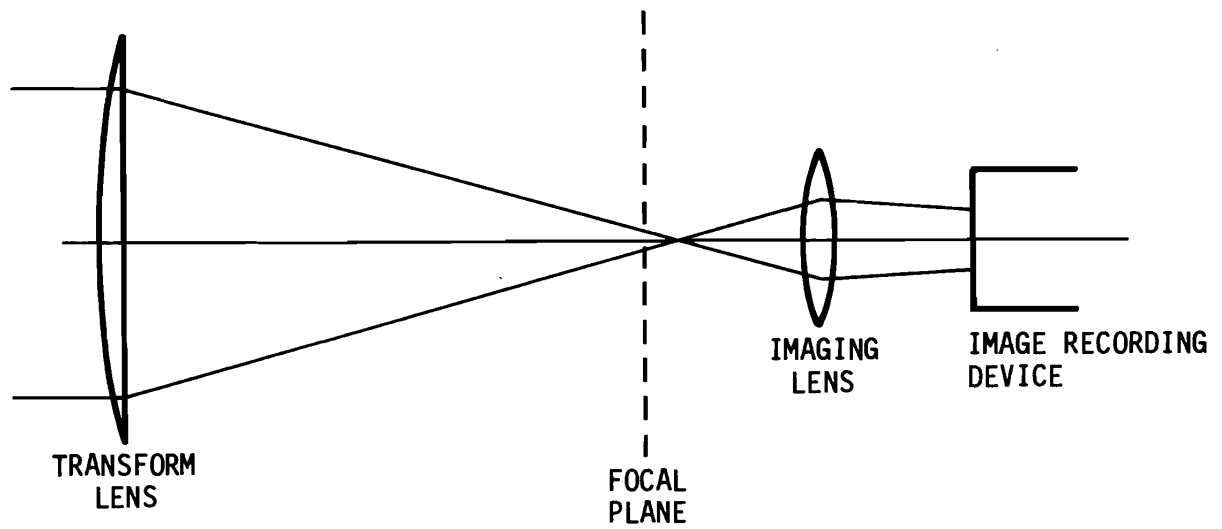


Figure 7-1. Image recording with the focal plane transform technique. With a second lens, the focal plane irradiance distribution is imaged with magnification on a suitable recording device.

8. SUMMARY

The preceding sections represent an attempt to illuminate the problem of far-field laser beam profile measurements from the point of view of measurement quality. They are not intended to dictate measurement technique or define parameters. Rather, we hope to have made clear the fact that measurement requirements evaluated with a knowledge of various trade-offs must determine the details of the measurement system and, accordingly, the quality of measurement.

To improve our ability to make such judgments, we have examined in some detail the consequences of a particular choice of measurement parameters for a particular quality to be measured. The results show that for this particular set of conditions measurements of generally acceptable accuracy (less than $\sim 10\%$) are possible with reasonable care. We urge caution, however, in applying this result to measurement systems with different parameters or to beams with substantially different characteristics. This specific analysis should be used, instead, to illustrate the nature of parameter choices and their effect.

The greatest advantage of using focal plane measurements to obtain far-field characteristics is simplicity. We can suggest no comparably simple technique of any sort. The greatest disadvantage of this technique is the possibility that, without sufficient care, substantially erroneous measurements can be obtained.

9. REFERENCES

- [1] Goodman, J. W., Introduction to Fourier Optics (McGraw-Hill Book Co., Inc., New York, N.Y., 1968).
- [2] Cathey, W. T., Optical Information Processing and Holography (John Wiley, New York, N.Y., 1974).
- [3] Collier, R. J., Burckhardt, C. B., and Lin, L. H., Optical Holography (Academic Press, New York, N.Y., 1971).
- [4] See Chapter 5 of Reference [2] for greater detail.
- [5] Siegman, A. E., An Introduction to Laser and Masers, Chapter 8 (McGraw-Hill Book Co., Inc., New York, N.Y., 1971).
- [6] Yariv, A., Quantum Electronics, Chapter 14 (John Wiley, New York, N.Y., 1967).
- [7] Kruger, J. S. Beam Divergence for Various Transverse Laser Modes, Harry Diamond Laboratories Report HDL-TM-71-11, AD 729 299 (1971).
- [8] Jenkins, F. A. and White H. E., Fundamentals of Optics, 4th Edition (McGraw Hill Book Co., Inc., New York, N.Y., 1976).
- [9] Klein, M. V., Optics (John Wiley, New York, N.Y., 1970).
- [10] Bieberman, L. M. and Nudelman, S., Editors, Photoelectronic Imaging Devices, Vol. 2 (Plenum Press, 1971).
- [11] Jahnke, E. and Emde, F., Tables of Functions with Formulae and Curves, p. 149, 4th Ed. (Dover, New York, N.Y., 1945).
- [12] Erdelyi, A., Higher Transcendental Functions, Eq. (52), p. 95, Vol. 2 (McGraw-Hill Book Co., Inc., New York, N.Y., 1953).

10. ACKNOWLEDGMENT

This work was supported by the Air Force Guidance and Metrology Center, Newark Air Force Station, Ohio, and by the Department of Defense Calibration Coordination Group through its Laser and Infrared Working Group.

APPENDIX

In the field of optics, when Fourier transform techniques are applied to obtain diffraction relations, approximations are usually made which lead to expressions valid in the Fresnel region and beyond. As a background to section 2, we present here a derivation of the Fresnel-Kirchhoff diffraction integral (2-3) using the Fourier transform approach without any small angle approximations. The approach is essentially that of Collier, et al. [3].

Using the notation of section 2.1 we write

$$\begin{aligned} U_2(x_2, y_2) &= F^{-1}\{\hat{U}_1(\xi, \eta) \exp[ikz(1-\lambda^2\xi^2-\lambda^2\eta^2)^{\frac{1}{2}}]\} \\ &= U_1(x_1, y_1) \times F^{-1}\{\exp[ikz(1-\lambda^2\xi^2-\lambda^2\eta^2)^{\frac{1}{2}}]\} \end{aligned}$$

where \times denotes convolution.

The inverse transform can be written

$$F^{-1}\{ \} = \int_{-\infty}^{\infty} \int_{-\infty}^{\infty} \exp[ikz(1-\lambda^2\xi^2-\lambda^2\eta^2)^{\frac{1}{2}}] \exp[i2\pi(\xi x + \eta y)] d\xi d\eta.$$

Making the transforms

$$\begin{aligned} \xi &= \rho \cos \alpha & x &= r \cos \phi \\ \eta &= \rho \sin \alpha & y &= r \sin \phi \end{aligned}$$

we obtain

$$F^{-1}\{ \} = \int_0^{\infty} \exp[ikz(1-\lambda^2\rho^2)^{\frac{1}{2}}] \rho d\rho \int_0^{2\pi} \exp[i2\pi r \rho \cos(\alpha-\phi)] d\alpha.$$

The integral over α is evaluated using the formula [11]

$$J_n(z) = \frac{i^{-n}}{2\pi} \int_0^{2\pi} e^{iz \cos \phi} e^{in\phi} d\phi \quad (n=0)$$

yielding

$$F^{-1}\{ \} = 2\pi \int_0^{\infty} \exp[ikz(1-\lambda^2\rho^2)^{\frac{1}{2}}] J_0(2\pi r \rho) \rho d\rho.$$

The integral over ρ is evaluated using the formula [12]

$$\begin{aligned} \int_0^{\infty} J_0(bt) \exp[-a(t^2-y^2)^{\frac{1}{2}}] (t^2-y^2)^{-\frac{1}{2}} t dt \\ = \exp[-iy(a^2+b^2)^{\frac{1}{2}}] (a^2+b^2)^{-\frac{1}{2}} \end{aligned}$$

which is differentiated with respect to a to obtain

$$\int_0^{\infty} J_0(bt) \exp[-a(t^2 - y^2)^{1/2}] t dt$$

$$= \exp[-iy(a^2 + b^2)^{1/2}] \left[\frac{a}{a^2 + b^2} \right] \left[\frac{1}{(a^2 + b^2)^{1/2}} + iy \right].$$

The inverse transform can then be written

$$F^{-1}\{ \} = \frac{-ikz}{2\pi} \frac{\exp[-ik(z^2 + r^2)^{1/2}]}{(z^2 + r^2)} \left[1 + \frac{1}{ik(d^2 + r^2)^{1/2}} \right].$$

For d greater than a few wavelengths, the second term in brackets is clearly much less than one so the transform becomes

$$F^{-1}\{ \exp[ikz(1 - \lambda^2 \xi^2 - \lambda^2 \eta^2)^{1/2}] \} = \frac{-ikz}{2\pi} \frac{\exp[-ik(z^2 + r^2)^{1/2}]}{(z^2 + r^2)}.$$

Now performing the convolution indicated above and writing r explicitly in terms of x and y , we have

$$U_2(x_2, y_2) = \frac{z}{i\lambda} \int_{-\infty}^{\infty} \int_{-\infty}^{\infty} U_1(x_1, y_1) \frac{\exp[-ik(z^2 + (x_2 - x_1)^2 + (y_2 - y_1)^2)^{1/2}]}{[z^2 + (x_2 - x_1)^2 + (y_2 - y_1)^2]} dx_1 dy_1$$

which is the diffraction integral we set out to obtain.

4. TITLE AND SUBTITLE Laser Far-Field Beam-Profile Measurements by the Focal Plane Technique		5. Publication Date March 1978	6. Performing Organization Code 276.01
7. AUTHOR(S) G. W. Day and C. F. Stubenrauch		8. Performing Organ. Report No.	
9. PERFORMING ORGANIZATION NAME AND ADDRESS NATIONAL BUREAU OF STANDARDS DEPARTMENT OF COMMERCE WASHINGTON, D.C. 20234		10. Project/Task/Work Unit No. 2761171	11. Contract/Grant No.
12. Sponsoring Organization Name and Complete Address (Street, City, State, ZIP) Air Force Guidance and Metrology Center, Newark Air Force Station, Ohio and Department of Defense CCG, Laser and Infrared Working Group		13. Type of Report & Period Covered	14. Sponsoring Agency Code
15. SUPPLEMENTARY NOTES			
16. ABSTRACT (A 200-word or less factual summary of most significant information. If document includes a significant bibliography or literature survey, mention it here.) An analysis of laser far-field beam-profile measurements by the focal plane technique is given. Particular attention is paid to systems at $\sim 1\mu\text{m}$ wavelength and having apertures up to 10 cm. The basic mathematics is reviewed and approximations are evaluated. Using geometrical optics techniques, it is shown that an f/20 plano-convex lens is an appropriate choice for the focusing element. For two arbitrarily chosen laser beam profiles the errors associated with the choice of this lens are discussed through the use of computed far-field and focal-plane irradiance distributions. Experimental procedures including methods of testing the optical elements are also given.			
17. KEY WORDS (six to twelve entries; alphabetical order; capitalize only the first letter of the first key word unless a proper name; separated by semicolons) Beam divergence; beam profile; lasers; optical propagation.			
18. AVAILABILITY <input type="checkbox"/> Unlimited <input type="checkbox"/> For Official Distribution. Do Not Release to NTIS <input checked="" type="checkbox"/> Order From Sup. of Doc., U.S. Government Printing Office Washington, D.C. 20402, SD Cat. No. C13.46:1001 <input type="checkbox"/> Order From National Technical Information Service (NTIS) Springfield, Virginia 22151		19. SECURITY CLASS (THIS REPORT) UNCLASSIFIED	21. NO. OF PAGES 52
		20. SECURITY CLASS (THIS PAGE) UNCLASSIFIED	22. Price \$2.20